Anonymous Referee #1

* General comments

The authors have measured rBC mass concentrations, size distributions and mixing states at a remote site on the south-east Tibetan Plateau with a single particle soot photometer. The results are interesting but there are a number of potential issues with the measurements that don't seem to have been addressed, and a number of conclusions are reached without sufficient supporting evidence. Therefore, I have many comments that I believe must be addressed before the manuscript is considered for publication in ACP.

Response: We appreciate the reviewer's thoughtful and valuable comments. We have made most of the changes suggested by the reviewer, both to the text and figures.

Consiceness is generally a problem. For example, the point that pollution can be transported to the Tibetan Plateau from the south through valleys is made multiple times in different locations with different types of supporting evidence. The consiceness of the manuscript could be improved considerably by making this point only once, with all of the supporting evidence raised at the same time. For example, Figs. 6c and the MODIS images in Fig. S5 make essentially the same point. Why are they discussed at different points in the manuscript?

Response: The purpose of showing the MODIS images in Fig. S5 was to show that pollutants (including rBC) from the IGP and Bangladesh were likely transported to Lulang on the morning (08:00–10:00 LT) of sampling days. The Terra satellite passed over the TP region at ~10:30 LT, and the timing of the overpass is within the observed morning peak in rBC. Thus, the MODIS images for the morning combined with the wind distributions are an effective way of illustrating regional transport for a specific case. In contrast, the BC column mass density in Fig. 6c was an average daily distribution for the entire campaign. As the CWT analysis was used for all of the trajectories during the entire campaign, the average daily distribution of BC column mass density was a way of showing the

region with high CWT values corresponded to the large BC loadings. In the revised manuscript, we deleted redundant expressions to make the paper more concise.

The large rBC concentrations measured on 21 October is an interesting observation and perhaps worthy of further investigation. Is it possible to link this to a specific event, to see if such events might occur frequently in this region? This is potentially important since the concentrations observed on this day seem to be ~4 times higher than the normal daily peak concentrations.

Response: Although the peak concentration of rBC on 21 October was much higher than the other days, its diurnal profile was similar to most of sampling days; that is, an increasing trend in rBC loadings occurred from 08:00–10:00 LT (see Fig. R1 below). As we discussed in the manuscript, the large morning peaks resulted from the combined effects of local activities and regional transport. Over short time-scales, such as the length of our study, the emission sources can be considered relatively stable. Thus, regional transport was thought to play an important role in this high rBC episode. The three-day backward trajectory analysis for 08:00–10:00 LT on 21 October show that the air parcel was over Guwahati, northeastern India, for a considerable time before arriving at Lulang (see Fig. R2 below). The amount of time the air masses spent over this anthropogenic region was likely sufficient for rBC particle loadings to build up, and it was these particles that were subsequently transported to Lulang. In the revised manuscript, we added the following: "It should be noted that even though the average rBC concentration from 08:00–10:00 on 21 October was ~8 times higher than the average value for other sampling days, the diurnal pattern of 21 October was similar to that seen on other days (Fig. S8a). Indeed, the rBC diurnal loading pattern did not appear to different on this high rBC concentration day (Fig. S8 b and c). Over short time scales, such as the length of our study, one can assume that the local emission sources are relatively stable. Based on the three-day backward trajectory analysis, sudden high rBC loadings such as those on the morning on 21 October may be explained by the slow passage of air over Guwahati

in northeastern India (Fig. S9). Large numbers of rBC particles likely accumulated in the air as it slowly passed over this polluted region, and it was those particles that were eventually transported to Lulang."

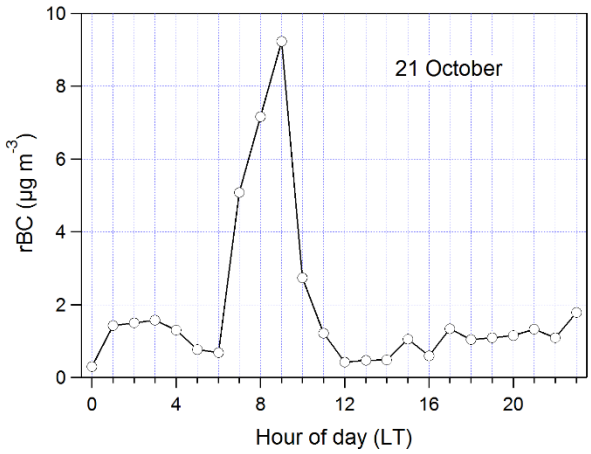

Figure R1. Diurnal variation of rBC mass concentrations on 21 October, 2015

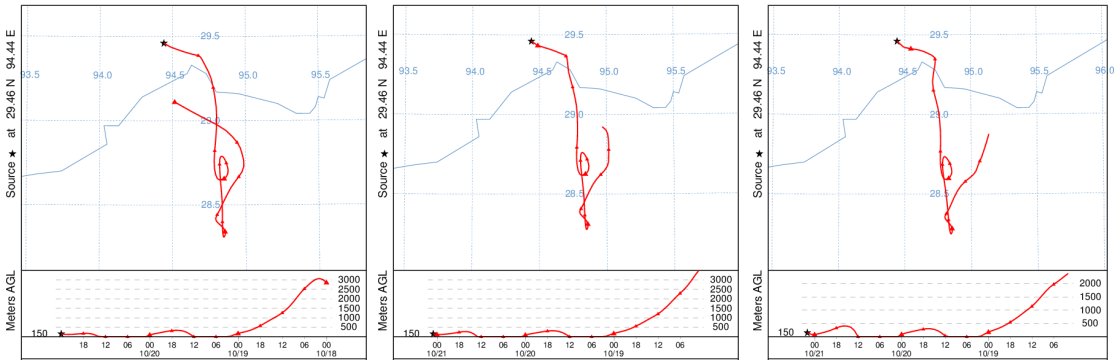

Figure R2. Three-day air-mass trajectories calculated backwards in time for 08:00–10:00 (local time) on 21 October 2015.

There are still a number of grammatical errors in the manuscript and sentences that should be split into smaller parts. I have tried to point these out in my specific comments below but I cannot guarantee that this is an exhaustive list. Further proof-reading is required.

Response: In some cases, long sentences are the most effective way of showing relationships among complex concepts, but we have tried to split long sentences into shorter ones. The paper also has been further proofed by a native English speaker.

* Specific comments

P2, L2: Split the sentence in 2. E.g. '...high-elevation region. It holds ..'

Response: Change made. It now reads: "The Tibetan Plateau (TP) is the world's largest high-elevation region. It holds the largest ice mass on the planet outside the polar regions and is sometimes called the Earth's "Third Pole" (Yao et al., 2008)."

P2, L23: Split the sentence. E.g. '...BC sources are strong (). The TP has become impacted...'

Response: Change made. It now reads: "Geographically, the TP is surrounded by South and East Asia where BC sources are strong (Zhang et al., 2009), and the TP has become impacted by these high-BC source areas due to the general circulation patterns (Cao et al., 2010; Lu et al., 2012; Zhao et al., 2017)."

P2, L26: Split the sentence. E.g. '...of surrounding areas. Annually, on average, South and East...'

Response: Change made. It now reads: "For example, Lu et al. (2012) found that BC loadings in the Himalayas and TP increased by 41% from 1996 to 2010 due to the influences of surrounding areas. Annually, on average, South and East Asia account for 67% and 17% of BC transported to the plateau, respectively."

P3, L4: Artifact should be changed to artefact. And this sentence appears to be conflating two separate concepts. The bulk collection of particles on filters is a design choice, not a measurement artefact. E.g. particles could be classified by size before they are collected on filters. Measurement artefacts are errors arising from the measurement technique itself, e.g. the filter loading effect.

Response: There is some debate regarding the usage of artifact vs. artifact, but a substantial number of online sources indicate that the difference is just between British vs. American English. Even so, we have made this change. Some online or offline filter-based techniques (e.g., aethalometer and multi-angle absorption

photometer) typically obtain BC mass at a specific size based on the inlet cyclone cutoff diameter. Although cascade impactors have been used to collect size-segregated aerosol samples for BC analysis, these instruments can only obtain data for several size ranges. In order to make this clearer, we revised this sentence in the revised manuscript. It now reads: "Although some aerosol-related field studies have been conducted on the TP, the BC measurements were mainly made using online or offline filter-based techniques (e.g., aethalometer, thermal/optical reflectance method, and multi-angle absorption photometer) (e.g., Engling et al., 2010; Marinoni et al., 2010; Wan et al., 2015; Zhu et al., 2016; Li et al., 2017). These techniques are based on the bulk particle deposition onto the filters, and they cannot provide high time resolution information on BC size and mixing state."

P3, L11: 'in' missing between 'change' and 'absorption'.

Response: Change made. It now reads: "That study showed that BC particles initially changed from a fractal to spherical morphology with little change in absorption followed by growth into compact particles with large E_{abs}."

P3, L19: This is not consistent with general practice in the field. E.g. BC mass calculated from measured light absorption is called equivalent BC (eBC), not simply BC (Petzold et al., 2013).

Response: In the revised manuscript, we changed this sentence to "Here the term rBC is used exclusively in reference to SP2 measurements while eBC (equivalent BC) and EC (elemental carbon) refer to the data from the optical absorption method and the thermal heating and optical absorption techniques, respectively, used in other studies (Petzold et al., 2013)."

P3, L25: This sentence requires re-wording. What sort of samples? The sentence should also be split. The free-troposphere part deserves its own sentence. Under what conditions are free troposheric air masses sampled at the site?

Response: Previous studies based on meteorological analysis have identified the Tibetan Plateau and the Himalayas as global hot spots for deep stratosphere-to-

troposphere transport (e.g., Škerlak et al., 2014). Moreover, measurements in those areas can at times reflect the composition of free tropospheric air. As it was beyond the scope of our study to identify the conditions that would lead to the sampling tropospheric air, we revised this text to, "Physicochemical and optical properties of rBC aerosol were measured in samples collected from a remote area of Lulang, which is located on the southeastern part of the TP (Fig. 1). An intensive measurement campaign was conducted from 17 September to 31 October 2015 on the dormitory rooftop of the Integrated Observation and Research Station for Alpine Environment in South-East Tibet, Chinese Academy of Sciences (94.44°E, 29.46°N, ~3300 m above sea level)."

Reference:

Škerlak, B., Sprenger, M., and Wernli, H.: A global climatology of stratosphere–troposphere exchange using the ERA-Interim data set from 1979 to 2011, Atmos. Chem. Phys., 14, 913–937, doi:10.5194/acp-14-913-2014, 2014.

P4, L6: It should also be mentioned that the SP2 detects elastically scattered light as well as thermal radiation, since the 'scattering signal' is discussed later in the discussion of how SP2 provides mixing state information.

Response: Following the reviewer's suggestion, we added the following in the revised manuscript: "Simultaneously, the laser light scattered by the rBC-containing particle was detected elastically."

P4, L21: It is not clear how the 20% uncertainty estimate has been arrived at. Please provide further quantitative details. Was the 'SP2 response to ambient rBC mass' determined from an independent measurement of BC mass?

Response: The SP2 needs an empirical calibration to retrieve the rBC mass from the incandescence signal, and the sensitivity of the SP2 differs among BC particle types. Ideally, for atmospheric studies, the SP2 should be calibrated using ambient particles containing a known mass of rBC. However, such "ambient BC" calibration particles cannot easily be obtained. Thus, commercially available BC

particles are commonly used for SP2 calibration instead. In the study of Laborde et al. (2012), the sensitivity of the SP2 to different BC types was tested to characterize the potential error introduced by using non-ambient BC for calibration. We cited their results (~15%) as the uncertainty of the SP2 response to ambient rBC mass in our study. The propogated uncertainty of the SP2 measurement was estimated from the square root of uncertainties caused by the SP2 response to ambient rBC mass (~15%), sample flow (10%), and estimates of the rBC mass beyond of SP2 detection range (10%). In the revised manuscript, we revised the original sentence to "The uncertainty of the SP2 mass measurements was ~20%, which was estimated by propagating the uncertainties caused by the SP2 response to ambient rBC mass (~15%, Laborde et al., 2012), sample flow (10%), and estimates of the rBC mass beyond the SP2 detection range (10%)."

Reference:

Laborde, M., Mertes, P., Zieger, P., Dommen, J., Baltensperger, U., and Gysel, M.: Sensitivity of the Single Particle Soot Photometer to different black carbon types, Atmos. Meas. Tech., 5, 1031-1043, doi:10.5194/amt-5-1031-2012, 2012.

P5, L4: Fig. S1 does not show that the 'vast majority' of rBC particles had VED between 70 and 300 nm. The figure shows that at least approximately half of the rBC particles had VED less than 70 nm (possibly more since the peak of the dN/dlogDp curve has not been reached by 70 nm).

Response: We meant that the size range of 70–300 nm accounted for most of the detected rBC particles. Due to limitations of the SP2 measurements, we could not obtain data for rBC particles smaller than 70 nm. In the revised manuscript, we modified this sentence to "An examination of the number size distribution of rBC shows that this was not a critical limitation in the following analysis because that size range contained the vast majority of the detected rBC particles (see Fig. S1)."

P5, L8: Particle losses in such a Nafion tube (diameter 0.11 inches, length 48 inches) can be very large. Tubes of such small diameter are not typically used in aerosol

sampling lines. The authors should demonstrate to what extent particle losses may have affected the measured b_abs values.

Response: We conducted an experiment to compare the b_{abs} measured with and without the Nafion tube (Perma Pure MD-700 dryer). As shown in Fig. R3 below, the particle loss for this type of Nafion tube may be ~10%. Thus, the b_{abs} values were scaled up by a factor of ~1.1 to compensate for the losses. We have added this information in the revised manuscript.

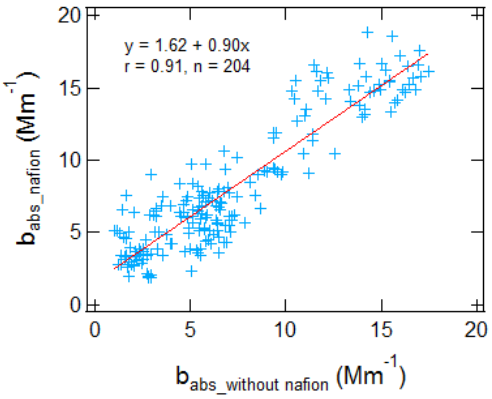

Figure R3. Scatter plot of light absorption coefficient measured with (b_{abs_nafion}) and without ($b_{abs\_without\ nafion}$) Nafion dryer (MD-110-48S).

P5, L15: b_ext values calculated in this manner require very large aerosol loadings due to the short 0.354 m optical path length in the PAX. The aerosol loadings used for the calibrations should be mentioned along with the range of ambient values measured, to give a sense of where the calibrations have been extrapolated to.

Response: In the revised manuscript, we added a Fig. S3 (also see Fig. R4 below) to show the results of PAX calibration. Following the reviewer's suggestion, we added the following in the revised manuscript: "Different concentration gradients of freshly-generated propane soot were used to give an absorption reading of ~10 to 16700 Mm^{-1} for absorption calibration (Fig. S3)."

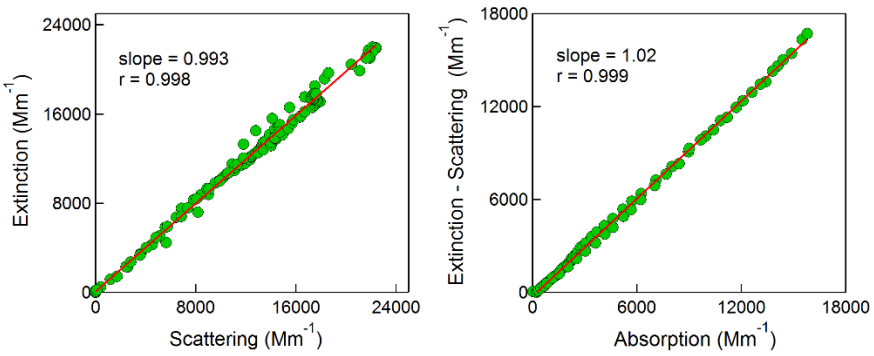

Figure R4. Scattering and absorption calibration of the photoacoustic extinctiometer (PAX_{870}).

P5, L24: Please provide details of how the ~15% measurement uncertainty has been arrived at for the PAX. Additionally, the PAX can have difficulty measruring low, ambient absorption levels accurately (e.g. < ~ 1 Mm^{-1}). Was a lower limit of detection/quantification used in this study?

Response: We re-analyzed the PAX data and discarded the data that had values < 1 Mm^{-1} (~15% of total number of b_{abs} measurements), and the results were changed accordingly in the revised manuscript. Moreover, we added the following text to clarify how the uncertainty obtained: "The uncertainty of the PAX for absorption measurements was estimated to be ~15% based on the variations of b_{abs} caused by the noise during the sampling period."

P6, L1: Please provide more details on the PBL depths that were used. Are they from a model? It is not clear which data were used by clicking through to the link provided.

Response: The PBL heights were simulated from the European Centre for Medium-range Weather Forecasts (ECMWF) model. One can download the PBL data directly from ERA-Interim (Jan. 1979–present) reanalysis datasets at http://apps.ecmwf.int/datasets. In the revised manuscript, we changed the original sentence to "The planetary boundary layer (PBL) heights were obtained from the European Centre for Medium-range Weather Forecasts (ECMWF). These can be downloaded from ERA-Interim (Jan. 1979–present) reanalysis datasets at http://apps.ecmwf.int/datasets."

P6, L19: It would be useful to discuss what this parameter means physically. I.e. positive values of f indicate ...

Response: Following the reviewer's suggestion, we added the following: "Positive values for f were considered indicative of transport from outside the TP (e.g., the Indo-Gangetic Plain, IGP, and Bangladesh) whereas negative values indicated transport from the interior of the TP."

P6, L25: Please provide further details about the actual clustering procedure that was used. Currently, only the calculation of the mean angle parameter d_12 is discussed. No information is provided about how this parameter was used to cluster back trajectories into different groups.

Response: Following the reviewer's suggestion, we added the following in the revised manuscript: "A two-step algorithm was used to produce the clusters. First, a Hartigan's K mean algorithm was used to construct several clusters of backward trajectories. Those clusters were then examined visually, and selected backward trajectories were moved from one cluster to another in order to define clusters that were easier to interpret with respect to geographical and/or anthropogenic source regions. In this study, three clusters were chosen as representative of the backward trajectory clusters. The simulation was conducted using the GIS-based TrajStat software (Wang et al., 2009)."

P7, L10: This sentence requires more precision. E.g. change to '...the rBC sources that potentially influenced the air sampled at Lulang'

Response: Following the reviewer's suggestion, we revised the sentence to: "A CWT model was used to construct the spatial distribution of the rBC sources that potentially influenced the air sampled at Lulang."

P7, L26: This is difficult to see in Fig. S3. I suggest plotting the frequency distribution on a log x-scale or maybe a reduced x-axis length to highlight this point.

Response: We have replotted Fig. S3 in the revised supporting information. The new Fig. S5 is shown below (Fig. R5):

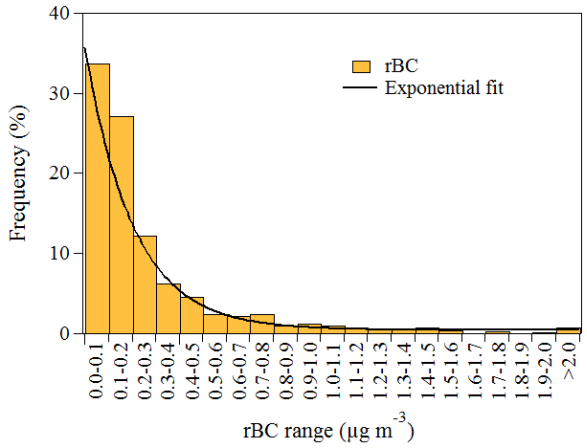

Figure R5. Frequency distribution of rBC mass concentrations during the campaign.

P9, L6: Were data from the 21 October included in the calculation of these diurnal profiles? I'm thinking if the apparent night time peak (or any other feature in the profile) was simply a result of this one-off event of high concentrations.

Response: In our original manuscript, the diurnal variations of rBC included the data from 21 October. As shown in Fig. R6 below, the diurnal pattern was similar with and without the data from 21 October. Following the reviewer's suggestion above, we have added some discussion about this high rBC episode in our revised manuscript. Please see the response above.

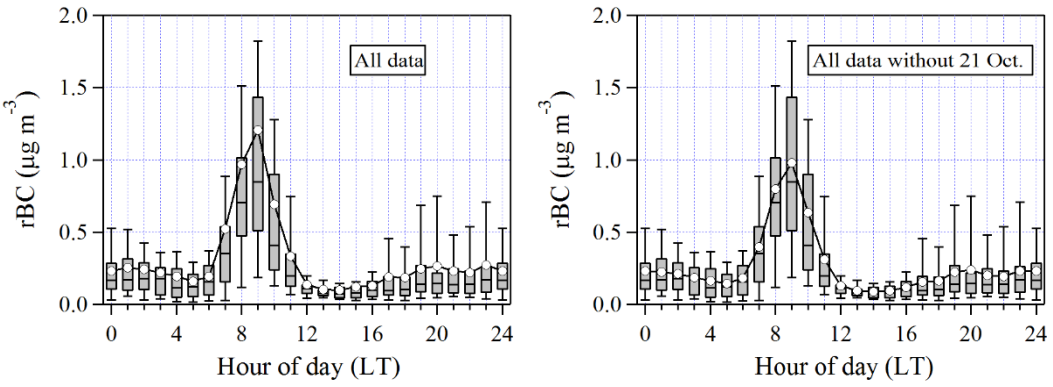

Figure R6. Diurnal variations of rBC with and without data from October 21.

P9, L18: Missing 'by' between 'accompanied' and 'deepening'.

Response: Change made. It now reads: "As shown in Fig. 3 (a–b), the rapid morning increases in rBC were accompanied by deepening of the PBL, which suggests the possibility that regional transport had an important influence on rBC particles."

P9, L27: Change 'south' to 'southern'.

Response: Change made. It now reads: "The true color images reveal obvious pollution bands along the IGP and Bangladesh that piled up on the southern margin of the TP."

P10, L14: While this is physically plausible, a statistical test should be conducted to determine whether it is really possible to say from this dataset that rBC concentrations were lower on moderate or heavy rain days than rBC concentrations on light rain days. Given the small sample size (only 4 moderate or heavy rain days), it may not be.

Response: A t-test for the rBC concentrations during light and strong rains showed that there was a statistically significant difference between them at a probability for chance occurrence of $p < 0.01$ ($p = 4.5 \times 10^{-6}$). We added a sentence to this effect in the revised manuscript. It reads "A t-test for the rBC concentrations during light and strong rains showed that there was a statistically significant difference between them at a probability for chance occurrence of $p < 0.01\%$."

P10, L15: Split the sentence. E.g. '... (Fast et al., 2007). Fig. 4a shows...'

Response: Change made. It now reads: "Wind speed and wind direction play crucial roles in the dilution and dispersion of pollutants (Fast et al., 2007). Fig. 4a shows the wind speeds and directions during the study."

P11, L30-35: While interesting, this is the 3rd time this observation has been mentioned. The consiceness of the manuscript could be improved considerably by making this point only once.

Response: In the revised manuscript, we deleted the redundant expressions to make the discussion more concise. Please see the new manuscript.

P12, L14: An 'and' is required between 'rural' and 'remote'.

Response: Change made. It now reads: "Fig. S1 shows that rBC core size distribution was well represented by a mono-modal lognormal fit. This is consistent with the size distributions constructed from previous SP2-based observations made across the globe, including urban, rural, and remote areas (e.g., Schwarz et al., 2008a; Liu et al., 2010; McMeeking et al., 2011; Huang et al., 2012; Wang et al., 2014)."

P12, L31: Please provide more explanation as to how air mass transport histories might affect rBC size distributions. I'm not aware of any mechanism by which rBC core VED (i.e. rBC mass) would change during transport (e.g. due to evaporation or condensation). Size-dependent removal processes could change the rBC core size distribution as discussed in the sentences following. In any case, the cluster analysis example that is given does not demonstrate that air mass transport histories affected the rBC size distributions. The rBC from the different source regions may simply have had different initial size distributions.

Response: The effects of air mass transport histories on the aerosol populations are mainly due to two things: one is where they originate, and the other is the effects of atmospheric processing during transport. We agree with the reviewer that different source regions may affect the initial size distributions of rBC. With reference to atmospheric processing, the growth of particles in ambient air can be affected by water accretion, coagulation, vapor condensation, and addition of materials formed through heterogeneous reactions. All of these can lead to rBC-containing particle growth as measured by aerodynamic size. However, only the process of coagulation can make the "rBC core" in a particle grow, i.e., increase the rBC in VED. In the revised manuscript, we changed the original expression to make this clear. It now reads: "Second, transport histories matter because aging of

the particles can affect the size distributions of rBC. Take the cluster analysis as an example: the average rBC MMD was the largest (184 ± 17 nm) when the polluted air masses originated from central Bangladesh (Cluster #2). In contrast, smaller rBC MMDs were found when the polluted air masses came from North India (Cluster #1, 173 ± 26 nm) or the central TP (Cluster #3, 177 ± 19 nm). These air masses originated from different source regions, and they may have had different rBC sizes initially; but the rBC core sizes also may have changed during transport through coagulation. It should be noted that a t-test for the rBC MMDs from different clusters showed that there was a statistically significant difference between Cluster #1 and #2 ($p < 0.01$), but was not significant between Cluster #2 and #3 ($p = 0.09$)."

P13, L10: Two things could explain the observed differences in Fig. 7: the absence of long-range transport during the rainy days or preferential wet scavenging of larger rBC cores during the rainy days. For the 2nd hypothesis, could the authors provide a reference or further theoretical argument to indicate whether this is feasible?

Response: Following the reviewer's suggestion, we revised the original expression to "Compared with non-rainy days, the smaller rBC on rainy days can be explained by the absence of long-range transport and by the preferential wet scavenging of larger rBC cores (Taylor et al., 2014)."

P13, L31: Photochemical production of coating material is just one explanation for the increased F_rBC during the afternoon. Mixing layer height was also high during the afternoon. Comparison of Fig. 3 and Fig. 8 suggests F_rBC also correlated well with mixing layer height for the periods from 10:00-19:00. Thus, another potential explanation for the high F_rBC values observed in the afternoon is the mixing of more aged BC particles from aloft to the surface.

Response: We added this possible explanation in the revised manuscript: "Moreover, the variations in F_{rBC} during the daytime at Lulang also covaried with

the PBL heights, indicating that aged rBC particles may have been transported from aloft to the surface."

P13, L32: I don't think it has been demonstrated that in situ photochemisty is completely responsible for the afternoon increase in F_rBC (see above comment). Therefore, I don't think it is justified to report oxidation rates and compare such rates with those observed at Qinghai Lake.

Response: As we were not able to quantify the effects of aged rBC particles throughout the column, we deleted the discussion of the oxidation rates in the revised manuscript.

P14, L20: The PAX can have difficulties to measure b_abs values less than ~1 Mm^{-1}. Since a considerable amount of the measurements fall in this range, could the authors provide a scatterplot of b_abs vs rBC concentrations from the SP2, and if relevant add it to the supplementary information? Such a plot might help to determine if a lower limit of quantification should be applied to the PAX measurements. E.g. if it shows the PAX was insensitive to changes in BC concentration below some threshold.

Response: We reanalyzed the PAX data. There was no correlation between b_{abs} and rBC mass concentrations when b_{abs} values less than 1 Mm^{-1}. During our sampling period, ~15% of total number of b_{abs} observations was lower than the minimum detection limit of 1.0 Mm^{-1}. These data were excluded in the revised manuscript. We have added this information in our revised Section 2.2.2, and the results in Section 3.5 (both text and figures) also has been reworked accordingly.

P14, L26: Given the very narrow nafion drier used in front of the PAX, I think it must be checked whether the b_abs measurements are biased low, which would mean these MAC values are also biased low.

Response: As shown in Fig. R3 above, this type of nafion dryer may cause ~10% of the loss for light-absorbing particles. In the revised manuscript, the values of b_{abs} were scaled up by a factor of ~1.1 to compensate for the losses, and the results in Section 3.5 (both text and figures) has been reworked accordingly.

P15, L12: Should be '... if the fraction of thickly coated rBC particles increased by one percent...'

Response: Change made. It now reads: "This means that if the fraction of thickly-coated rBC particles increased by one percent, the rBC particles would absorb 3% more light."

P15, L25: More specifically, if coatings are formed by condensation, this is due to the 1/Diameter dependence of the condensation rate.

Response: We added this explanation in the revised manuscript. It now reads: "The variations in E_{abs} were relatively constant for rBC MMD > 170 nm. When coatings form by condensation, a 1/diameter dependence would apply to the condensation rate. Thus, larger rBC cores have smaller degree of internal mixing and weaker absorption amplification than smaller cores on the one hand, but on the other hand, larger rBC core size also would decrease the $MAC_{rBC,uncoated}$ according to the Mie model (see the relationship between $MAC_{rBC,uncoated}$ and MMD in Fig. S12)."

P16, Section 4: A number of the conclusions made in this section might need to be updated after the specific comments above have been addressed.

Response: We revised the conclusions accordingly. Please see the conclusion section in the revised manuscript.

References: Petzold, A., Ogren, J. A., Fiebig, M., Laj, P., Li, S.-M., Baltensperger, U., Holzer-Popp, T., Kinne, S., Pappalardo, G., Sugimoto, N., Wehrli, C., Wiedensohler, A. and Zhang, X.-Y.: Recommendations for reporting "black carbon" measurements, Atmos. Chem. Phys., 13(16), 8365–8379, doi:10.5194/acp-13-8365-2013, 2013.

Anonymous Referee #2

Totally this MS has been greatly improved. However, there are still some problems in the MS. Firstly, the English still need to be further improved. Some sentences are a little long and need to be cut into short sentences. Secondly, some inconsistent tenses exist in some sentences, please check carefully.

Response: We thank the reviewer for taking the time to review our manuscript. We have revised most of the long sentences to the shorter ones, and the tenses also have been checked carefully. The language has been further proofed by a native English speaker.

This study only cover less than two months in autumn of 2015. Due to radiative and atmospheric chemistry at study area should be different at other seasons, the conclusion of this study should be limited and the uncertainties need also be pointed out in the MS.

Response: In the revised manuscript, we added the following in the conclusion section to clarify the limitation and uncertainties caused by the short sampling period: "We should note that the sources, transport, and radiative effects of the rBC as well as atmospheric conditions likely vary in complex ways with season, and therefore the results from our study (in autumn) are not necessarily representative of other times of the year. Indeed, additional studies need to be conducted to determine how the rBC aerosol at our site and others changes with season."

Anonymous Referee #4

The author has made a sincere effort to improvise the manuscript relative to the previous version. However, there is still a scope to correct it grammatically, the tenses and apt usage of phrases. Below are the primary comments both technical and non- technical which the author can address to enhance the quality of the manuscript.

Response: We thank the reviewer for taking the time to review our manuscript.

Page 3 Line 13: It is not clear what high resolution measurements the author is talking, is it about time, space?

Response: The reference was to high time resolution measurements. In the revised manuscript, we revised this sentence to "Accurate information on the physicochemical characteristics of BC can improve our understanding of anthropogenic climate impacts on the TP, but there is still lack of high time resolution measurements on the size and mixing state of BC in this region."

Page 6 Line 18-19: Section 2.3.1 requires more justification how evaluation of surface flux intensity is an indication of regional transport.

Response: The transport of pollutants was markedly influenced by meteorological parameters, especially wind speed and wind direction. For local emission sources, wind can facilitate the dilution and dispersion of air pollutants. Strong winds obviously favor dispersion whereas weak winds often lead to the accumulation of air pollutants. For regional sources, strong winds can transport pollutants over long distances, and that can lead to high concentrations of pollutants in downwind areas. If regional transport carried large rBC particles due to high winds, then the calculated surface flux intensity would be large. Therefore, in our study, we viewed the surface flux intensity as a measure of the influence of regional transport in South Asia, and more specifically on the Lulang site using ground-based observations. In the revised manuscript, we added the following text to make it clearer: "Generally, strong winds favor the dispersion of air pollutants for local emission sources whereas weak winds lead to accumulation. In contrast, for

regional sources, strong winds can transport pollutants from upwind areas and cause high concentrations of pollutants downwind. Therefore, in this study, we viewed the surface flux intensity as a measure of the influence of regional transport in South Asia, and more specifically on the Lulang site using ground-based observations."

Page 8 Line 31: Please elaborate few difficulties in obtaining scaling factors

Response: Actually, the difficulties in obtaining scaling factors were discussed in our original manuscript; these include the uncertainties caused by the inherent differences instruments themselves and a lack of BC method intercomparisons. This may have been misunderstanding of our original expression, and in the revised manuscript, we changed the sentence to "Therefore, limitations such as those mentioned above make it difficult to establish scaling factors to reconcile the various BC measurements on the TP to a common standard, and direct comparisons of BC data obtained by different methods can be tenuous."

Page 9 Line 1: i) "Fig 3 (a-c) shows the diurnal variations of rBC mass. . .." Please specify it as the averaged values over the entire campaign. ii) "PBL height" or "PBL depth", check and change throughout the manuscript iii) ..wind speed during the (not over the) entire campaign – check grammatical errors.

Response: We revised this sentence in the revised manuscript. It now reads: "Fig. 3 (a–c) shows the diurnal variations of the average rBC mass concentrations, PBL heights, and wind speeds during the campaign." We also changed all the "PBL depth" to "PBL height" throughout the manuscript.

Line 17: "As shown in Fig. 3 (a–b), the rapid morning increase in rBC was accompanied deepening of the PBL, and therefore, regional transport maybe an important influence on the aerosol populations." The meaning of this sentence is not clear. Reframe the sentence, and what is aerosol populations?

Response: The "aerosol populations" means different chemical components, such as rBC, organic aerosol, sulfate, nitrate, etc. However, since our study focused on

rBC aerosol, in order to make it more clear, we changed the "aerosol populations" to "rBC particles" in the revised manuscript. We reframed this sentence to "As shown in Fig. 3 (a–b), the rapid morning increases in rBC were accompanied by deepening of the PBL, which suggests the possibility that regional transport had an important influence on rBC particles."

Line 21: "After sunrise, as the PBL starts to deepen, strengthening thermals lift and eventually break the nighttime inversion, and this can lead to the transport of pollutants to the southeastern TP." Reframe the sentence, as PBL expansion is one of the important factor, but not the only factor

Response: In the revised manuscript, we revised this expression to "After sunrise, as the PBL starts to deepen, strengthening thermals lift and eventually break up the nighttime inversion. These changes in the atmosphere provide conditions that could support the transport of pollutants to the southeastern TP."

Line 30: In this sentence, "The decreasing trend in the late morning. . ." this change in rBC can well explained using wind direction. Was there any change in wind direction?

Response: The prevailing wind directions changed from southwest at 07:00–09:00 to northeast at 10:00–12:00. In the revised manuscript, we added the wind direction discussion. It now reads: "The decreasing trend in rBC loadings in the late morning at Lulang is consistent with the continued deepening of the PBL (Fig. 3b) and the strengthening winds from the northeast (see Fig. 2 and Fig. 3c)."

Page 12 Line 13: "Fig. S1 shows that rBC core size distribution was well represented by a mono-modal lognormal fit, which is consistent with previous SP2-based observations made across the globe, including urban, rural, remote areas". Consistent with respect to what? Can you further elaborate?

Response: We revised this sentence in the revised manuscript. It now reads: "Fig. S1 shows that rBC core size distribution was well represented by a mono-modal lognormal fit. This is consistent with the size distributions constructed from previous SP2-based observations made across the globe, including urban, rural,

and remote areas (e.g., Schwarz et al., 2008a; Liu et al., 2010; McMeeking et al., 2011; Huang et al., 2012; Wang et al., 2014)."

Page 13 Line 1-3: "In contrast, smaller rBC MMDs were found when the polluted air masses came from North India (Cluster #1, 173 nm) or central TP (Cluster #3, 177 nm). Moreover, more aged particles in the plumes tend to be larger than fresher particles from close to the source (Moteki et al., 2007)". So what is the significance of this? Yes aged particle will grow and will be typically larger than fresh ones... What is the std deviation of these mean value? The stated differences are hard to justify (meaning not significant) without the variation in the mean value?

Response: Here we used the results of cluster analysis as a way of demonstrating that air mass transport histories can affect the size distributions of rBC among different rBC studies. This is because the air masses that originate from different regions can have dissimilar initial rBC size distributions due to their main emission sources, etc. In addition, the rBC core sizes may be changed through coagulation during transport. We added the standard deviation of the mean MMD value for each cluster. We also used t-tests to determine whether there were statistically significant differences in the MMDs from different clusters. In the revised manuscript, we reworked this part. It now reads: "Second, transport histories matter because aging of the particles can affect the size distributions of rBC. Take the cluster analysis as an example: the average rBC MMD was the largest (184 ± 17 nm) when the polluted air masses originated from central Bangladesh (Cluster #2). In contrast, smaller rBC MMDs were found when the polluted air masses came from North India (Cluster #1, 173 ± 26 nm) or the central TP (Cluster #3, 177 ± 19 nm). These air masses originated from different source regions, and they may have had different rBC sizes initially; but the rBC core sizes also may have changed during transport through coagulation. It should be noted that a t-test for the rBC MMDs from different clusters showed that there was a statistically significant difference between Cluster #1 and #2 ($p < 0.01$), but was not significant between Cluster #2 and #3 ($p = 0.09$)."

Sources and physicochemical characteristics of black carbon aerosol from the southeastern Tibetan Plateau: internal mixing enhances light absorption

Qiyuan Wang[1*], Junji Cao[1,2*], Yongming Han[1,3], Jie Tian[4], Chongshu Zhu[1], Yonggang Zhang[1], Ningning Zhang[1], Zhenxing Shen[4], Haiyan Ni[1], Shuyu Zhao[1], and Jiarui Wu[1]

[1]Key Laboratory of Aerosol Chemistry and Physics, State Key Laboratory of Loess and Quaternary Geology, Institute of Earth Environment, Chinese Academy of Sciences, Xi'an, 710061, China
[2]Institute of Global Environmental Change, Xi'an Jiaotong University, Xi'an, 710049, China
[3]School of Human Settlements and Civil Engineering, Xi'an Jiaotong University, Xi'an, 710049, China
[4]Department of Environmental Sciences and Engineering, Xi'an Jiaotong University, Xi'an, 710049, China

Correspondence to: Junji Cao (cao@loess.llqg.ac.cn) and Qiyuan Wang (wangqy@ieecas.cn)

Abstract. Black carbon (BC) aerosol has important effects on the climate and hydrology of the Tibetan Plateau (TP). An intensive measurement campaign was conducted at Lulang (~3300 m above sea level), southeastern TP, from September to October 2015, to investigate the sources and physicochemical characteristics of refractory BC (rBC) aerosol. The average rBC mass concentration was 0.31 ± 0.55 μg m^{-3}, which is higher than most prior results for BC on the TP. A clear diurnal cycle in rBC showed high values in the morning and low values in the afternoon. A bivariate polar plot showed that rBC loadings varied with wind speed and direction, which also reflected the dominant transport direction. The estimated net surface rBC transport intensity was +0.05 ± 0.29 μg s^{-1} m^{-2}, indicating stronger transport from outside the TP compared with its interior. Cluster analysis and a concentration-weighted trajectory model connected emissions from north India to the high rBC loadings, but the effects of internal TP sources should not be overlooked. The average mass median diameter (MMD) of rBC was 160 ± 23 nm, with smaller MMDs on rainy days (145 nm) compared with non-rainy days (164 nm). The average number fraction of thickly-coated rBC (F_{rBC}) was 39 ± 8%, and it increased with the O_3 mixing ratios from 10:00–14:00, indicating that photochemical oxidation played a role in forming rBC coatings. The average rBC absorption enhancement (E_{abs}) was estimated to be 1.9, suggesting that light absorption by coated rBC particles was greater than for uncoated ones. The E_{abs} was strongly positively correlated with the F_{rBC}, indicating an amplification of light absorption for internally-mixed rBC. For rBC cores < 170 nm, E_{abs} was negatively correlated with MMD, but it was nearly constant for rBC cores > 170 nm. Our study provides insight into the sources and evolution of rBC aerosol on the TP, and the results should be useful for improving models of the radiative effects of carbonaceous aerosols in this area.

删除的内容: in
删除的内容: over the Tibetan Plateau (TP)
删除的内容: regional
删除的内容: ical
删除的内容: processes
删除的内容: grand
删除的内容: BC
删除的内容: were affected by
删除的内容: and it was used to infer the
删除的内容: s
删除的内容: for rBC
删除的内容: that
删除的内容: the
删除的内容: of the TP
删除的内容: indicated that
删除的内容: had important contribution
删除的内容: cannot
删除的内容: and it was
删除的内容: size
删除的内容: enhanced
删除的内容: local time
删除的内容: the
删除的内容: n important
删除的内容: The slope of a linear regression of F_{rBC} versus O_3 was 0.44 % ppb^{-1}, which was higher than the value of 0.24 % ppb^{-1} observed at Qinghai Lake, northeastern TP, suggesting that the rBC particles at Lulang were more rapidly affected by internal mixing than those at Qinghai Lake.
删除的内容: 8
删除的内容: that
删除的内容: the
删除的内容: When
删除的内容: the
删除的内容: in
删除的内容: is
删除的内容: further modelling studies
删除的内容: precise
删除的内容: evaluating
删除的内容: forcing

1 Introduction

The Tibetan Plateau (TP) is the world's largest high-elevation region. It holds the largest ice mass on the planet outside the polar regions and is sometimes called the Earth's "Third Pole" (Yao et al., 2008). The snow and associated glacial meltwater on the TP provides fresh water for drinking and irrigation for more than 1 billion people downstream (Immerzeel et al., 2010). The TP exerts significant thermal and dynamic impacts on hydrological processes in South and East Asia. For example, changes in the area covered by glaciers and snowpacks on the TP affect the heat fluxes and water exchange between the atmosphere and the earth's surface, and that, in turn, affects the atmospheric circulation associated with the Asian Monsoon System (Lau and Kim, 2006). Glaciers can be sensitive to climate change (Dyurgerov and Meier, 2000), and recent observations have shown a continuing retreat in Tibetan glaciers (e.g., Xu et al., 2009; Yao et al., 2012; Zhang et al., 2012; Loibl et al., 2014; Kang et al., 2015; Huintjes et al., 2016; Ke et al., 2017). For instance, Yao et al. (2012) reviewed the status of glaciers on the TP and surrounding areas over the past 30 years. These authors reported systematic differences from region to region, and their study showed that the greatest reduction in glacial length and area and the most negative mass balance occurred in the Himalayas (excluding the Karakorum).

The past few decades have witnessed rapid growth in the human population and industrialization in South and East Asia, and this growth has led to widespread air pollution (Vadrevu et al., 2014; Cao, 2017). An important component of this pollution is the black carbon (BC) aerosol, the light-absorbing, refractory material produced mainly through the incomplete combustion of fossil fuels and biomass (Bond et al., 2013). In addition to its effects on air quality, BC plays a unique and important role in the Earth's climate system due to its impacts on solar radiation, clouds, and snow albedo (Bond et al., 2013). Indeed, it has been suggested that BC is the second largest contributor to anthropogenic radiative forcing after carbon dioxide due to its strong absorption of solar radiation (Jacobson, 2001; Ramanathan and Carmichael, 2008; Bond et al., 2013). Furthermore, BC aerosol can alter atmospheric circulation patterns, accelerate snowmelt, and cause glaciers to retreat (Xu et al., 2009).

Geographically, the TP is surrounded by South and East Asia where BC sources are strong (Zhang et al., 2009), and the TP has become impacted by these high-BC source areas due to the general circulation patterns (Cao et al., 2010; Lu et al., 2012; Zhao S. et al., 2017). For example, Lu et al. (2012) found that BC loadings in the Himalayas and TP increased by 41% from 1996 to 2010 due to the influences of surrounding areas. Annually, on average, South and East Asia account for 67% and 17% of BC transported to the plateau, respectively. However, several recent studies showed that the impact of internal Tibetan sources (e.g., yak dung combustion by local residents) on the atmosphere of the TP should not be overlooked (Chen et al., 2015; Li et al., 2016a; Zhang X. et al., 2017). In the past few decades, a number of field campaigns conducted on the TP have investigated the concentrations, sources, and spatial and temporal variations of BC aerosol (e.g., Engling et al., 2011; Cong et al., 2015; Wang M. et al., 2016; Zhu et al., 2016; Wang et al., 2017; Zhao Z. et al., 2017). Recently, research has begun to focus on the light absorption characteristics of BC particles in the atmosphere and snow (Li et al., 2016b, 2016c; Zhang Y.et al., 2017). These studies have been helpful for improving estimates of the radiative forcing of BC in the atmosphere of the TP.

删除的内容: ,
删除的内容: and i
删除的内容: in
删除的内容: regions
删除的内容: respond sensitively
删除的内容: Li et al., 2016;
删除的内容: ,
删除的内容: and t
删除的内容: .
删除的内容: T
删除的内容: ,
删除的内容: , and urbanization over
删除的内容: Several studies
删除的内容:
删除的内容: ,
删除的内容: and
删除的内容: annual
删除的内容: ed
删除的内容: there
删除的内容: in
删除的内容:),
删除的内容: and t

Although some aerosol-related field studies have been conducted on the TP, the BC measurements were mainly made using online or offline filter-based techniques (e.g., aethalometer, thermal/optical reflectance method, and multi-angle absorption photometer) (e.g., Engling et al., 2011; Marinoni et al., 2010; Wan et al., 2015; Zhu et al., 2016; Li et al., 2017). These techniques are based on the bulk particle deposition onto the filters, and they cannot provide high time resolution information on of BC size and mixing state. This is a significant limitation of the filter-based methods because the optical properties of the BC aerosol are related to the particles' chemical and microphysical characteristics, including their size and mixing state. For instance, Liu et al. (2015) reported direct evidence of substantial field-measured BC absorption enhancement (E_{abs}) in an urban area, and this was strongly dependent on the internal mixing of BC. Peng et al. (2016) used a novel environmental chamber to quantify the aging and variations in the morphology and optical properties of BC particles from Beijing, China and Houston, United States. That study showed that BC particles initially changed from a fractal to spherical morphology with little change in absorption followed by growth into compact particles with large E_{abs}.

Accurate information on the physicochemical characteristics of BC can improve our understanding of anthropogenic climate impacts on the TP, but there is still lack of high time resolution measurements on the size and mixing state of BC in this region. This deficiency has led to considerable uncertainty in the calculations of BC direct radiative forcing over TP (He et al., 2014). In this study, we used a single-particle soot photometer (SP2) and a photoacoustic extinctiometer (PAX) to determine the mass concentrations, size distributions, mixing states, and light absorption properties of refractory BC (rBC) from the southeastern part of the TP. Various terms have been used in the literature for the most refractory and light-absorbing components of carbonaceous aerosols, and these have been based on the experimental measurement techniques (Bond et al., 2013). Here the term rBC is used exclusively in reference to SP2 measurements while eBC (equivalent BC) and EC (elemental carbon) refer to the data from the optical absorption method and the thermal heating and optical absorption techniques, respectively, used in other studies (Petzold et al., 2013). The primary objectives of this study were (1) to investigate the effects of meteorology on rBC and identify probable source regions responsible for the high rBC loadings; (2) to characterize the rBC size distributions and the evolution of rBC mixing state; and (3) to derive the rBC E_{abs} and evaluate the factors that affect it.

2 Methodology

2.1 Sampling site

Physicochemical and optical properties of rBC aerosol were measured in samples collected from a remote area of Lulang, which is located on the southeastern part of the TP (Fig. 1). An intensive measurement campaign was conducted from 17 September to 31 October 2015 on the dormitory rooftop of the Integrated Observation and Research Station for Alpine Environment in South-East Tibet, Chinese Academy of Sciences (94.44°E, 29.46°N, ~3300 m above sea level). There were no major anthropogenic sources near the sampling site.

删除的内容: 2010
删除的内容:
删除的内容: For t
删除的内容: artifacts result from
删除的内容: therefore,
删除的内容: the direct determination
删除的内容: with these techniques is infeasible
删除的内容: where the magnitude of E_{abs}
删除的内容: approach
删除的内容: lthough a
删除的内容: is needed
删除的内容: to
删除的内容: -
删除的内容: the
删除的内容: single
删除的内容: in
删除的内容: depending
删除的内容: more generally
删除的内容: s
删除的内容: measurements made with other
删除的内容: , and under the certain conditions samples air from the free troposphere

2.2 Data collection

2.2.1 Quantification of rBC mass, size, and mixing state

A single-particle soot photometer manufactured by Droplet Measurement Technologies (Boulder, CO, USA) was used to determine the mass, size, and mixing state of rBC particles. The operation and principles of the SP2 have been described in detail elsewhere (Schwarz et al., 2006). Briefly, a high-intensity intra-cavity Nd: YAG laser operating at wavelength of 1064 nm heats an individual rBC-containing particle to its incandescence temperature (~4000 K) which then emitted thermal radiation that was detected optically. Simultaneously, the laser light scattered by the rBC-containing particle was detected elastically. The intensity of the incandescence signal is proportional to the mass of rBC contained in the particle, but it is not affected by the particle morphology or the presence of non-refractory matter (Slowik et al., 2007). In this study, the SP2 was calibrated with a standard fullerene soot sample (Lot F12S011, Alfa Aesar, Inc., Ward Hill, MA, USA). A linear relationship was established between the peak intensity of the incandescence signal and the rBC mass. For this procedure, fullerene soot particles generated by an atomizer (Model 9302, TSI Inc., Shoreview, MN, USA) were passed through a diffusion silica-gel dryer, and then they were separated by size with a differential mobility analyzer (Model 3080, TSI Inc.) before entering the SP2 instrument. The corresponding fullerene soot masses were estimated using the effective density data provided by Gysel et al. (2011). More information concerning the SP2 calibration procedure may be found in Wang et al. (2014).

The measured rBC mass was converted to the volume equivalent diameter (VED) by assuming rBC particles were solid spheres with a density of 1.8 g cm^{-3} (Bond and Bergstrom, 2006). The detection efficiency of the SP2 drops off for rBC core sizes < ~70 nm, and the signal becomes saturated for sizes > ~600 nm. Based on a mono-modal lognormal fit for the mass size distributions as described in section 3.3.1 below (Supplemental Fig. S1), the reported rBC mass concentrations in this study were scaled up by a factor of ~1.1 to compensate the losses outside of the SP2 detection range. The uncertainty of the SP2 mass measurements was ~20%, which was estimated by propagating the uncertainties caused by the SP2 response to ambient rBC mass (~15%, Laborde et al., 2012), sample flow (~10%), and estimates of the rBC mass beyond the SP2 detection range (~10%).

A major advantage of the SP2 is that it has the capability of determining the rBC mixing state (Schwarz et al., 2006). Freshly emitted rBC can be internally mixed with non-rBC materials through the process of gas-to-particle conversion. When the laser beam in the SP2 heats an internally-mixed rBC particle, the coatings are preferentially evaporated, and that causes a decrease in the intensity of the scattering signal. After that, the rBC core starts to vaporize and that produces a peak in the incandescence signal. Therefore, there is a lag-time between the peaks of the scattering and incandescence signals. These lag-times can be used to characterize the internal mixing of rBC (McMeeking et al., 2011; Huang et al., 2012; Wu et al., 2016). Supplemental Fig. S2 shows that the lag-times exhibited a bimodal distribution with ~2 μs separating two distinct populations. The rBC-containing particles with a lag-time > 2 μs were considered to have substantial coatings, and those particles were denoted thickly-coated. In contrast, the rBC-containing particles with lag-times < 2 μs were classified as uncoated or thinly-coated. Here the number fraction of thickly-coated rBC (F_{rBC}) was used to represent the degree of internal mixing of the rBC particles,

删除的内容: n
删除的内容: SP2
删除的内容: emits
删除的内容: is
删除的内容: by
删除的内容: detectors
删除的内容: and
删除的内容: ,
删除的内容: and a
删除的内容: dropped
删除的内容: or
删除的内容: a
删除的内容: from
删除的内容: of
删除的内容: ,
删除的内容: ,
删除的内容: and that
删除的内容: was
删除的内容: are
删除的内容: the

and it was calculated by dividing the number of thickly-coated rBC particles by the total number of rBC particles. As there were no incandescence signals detected for small particles and the scattering signal became saturated for large coated rBC particles, the rBC core sizes used to evaluate internal mixing were limited to ~70 to 300 nm VED. An examination of the number size distribution of rBC shows that this was not a critical limitation in the following analysis because that size range contained the vast majority of the detected rBC particles (see Fig. S1).

2.2.2 Particle light absorption measurements

A photoacoustic extinctiometer, operating at wavelength of 870 nm (PAX_{870}, Droplet Measurement Technologies) was used to measure the particles' light absorption coefficients (b_{abs}) based on an intra-cavity photoacoustic technology. The light-absorbing particles were heated by the laser beam in the acoustic chamber. This heating produced a pressure wave that was detected with a sensitive microphone. The PAX_{870} can also measure the particles' light scattering coefficient (b_{scat}) simultaneously with a wide-angle integrating reciprocal nephelometer in the scattering chamber. Before and during sampling, the light scattering and absorption of the PAX_{870} were calibrated with ammonium sulfate and freshly-generated propane soot, respectively. The light extinction coefficient ($b_{ext} = b_{scat} + b_{abs}$) can be calculated from the laser power of the PAX_{870}. Thus a correction factor can be established from the relationship between the calculated b_{abs} ($= b_{ext} - b_{scat}$) and the measured b_{abs}. The b_{ext} is calculated using the following formula:

$$b_{ext} = -\frac{1}{0.354} \times \ln\frac{I}{I_0} \times 10^6 \ [Mm^{-1}] \quad (1)$$

where 0.354 is the path length of the laser beam through the cavity in meters; 10^6 is a conversion factor used to express b_{ext} in Mm^{-1}; I is the laser power during calibration (mW), and I_0 is the average laser power before and after calibration. A linear relationship was established between the extinction-minus-scattering coefficients and the measured b_{abs}. The slope of the regression line, that is, the correction factor, was then used as the new calibration factor for absorption. In this study, the same steps for the absorption calibration were repeated until the correction factor was stable within ~10%. Different concentration gradients of freshly-generated propane soot were used to give an absorption reading of ~10 to 16700 Mm^{-1} for absorption calibration (Fig. S3). The uncertainty of the PAX for absorption measurements was estimated to be ~15% based on the variations of b_{abs} caused by the noise during the sampling period. It is worth noting that the b_{scat} produced by freshly-generated propane soot particles has a substantial contribution to b_{ext} while ammonium sulfate is the only material that generates b_{scat}. Thus, the scattering was calibrated before the b_{abs} calibration using the same procedures as for the absorption calibration (Fig. S3). In this study, sampled particles passed through a Nafion® dryer (MD-110-48S; Perma Pure, Inc., Lakewood, NJ, USA) before entering the PAX_{870}. As shown in Supplemental Fig. S4, the light-absorbing particle loss for this type of Nafion tube may be ~10%. Thus, the b_{abs} values were scaled up by a factor of ~1.1 to compensate for the losses. Moreover, about 15% of

删除的内容: .
删除的内容: I
删除的内容: Because
删除的内容: ,
删除的内容: T
删除的内容: PAX
删除的内容: Sampled particles pass through a Nafion® dryer (MD-110-48S; Perma Pure, Inc., Lakewood, NJ, USA) before entering the PAX_{870}, and then
删除的内容: are
删除的内容: produces
删除的内容: is
删除的内容: ;
删除的内容: t
带格式的: 上标
删除的内容: is

total number of b_{abs} measurements was excluded because the values were lower than the minimum detection limit of PAX_{870} (1.0 Mm^{-1}).

2.2.3 Complementary data

A portable DustTrak™ aerosol monitor (Model 8530, TSI Inc., Shoreview, MN, USA) was used to measure the mass concentrations of total suspended particulate matter (TSP). Hourly ozone (O_3) was measured using a UV-based dual beam O_3 monitor (2B Technology model 205, CO, USA). Wind speed and wind direction were measured hourly with the use of an automatic weather station installed at the Integrated Observation and Research Station for Alpine Environment in South-East Tibet, Chinese Academy of Sciences. The planetary boundary layer (PBL) heights were obtained from the European Centre for Medium-range Weather Forecasts (ECMWF). These can be downloaded from ERA-Interim (Jan. 1979–present) reanalysis datasets at http://apps.ecmwf.int/datasets. The spatial distribution of the BC column mass density was retrieved from the Modern-Era Retrospective analysis for Research and Applications version 2 (MERRA-2) using the Goddard Earth Observing System Model, Version 5 (GEOS-5) with its Atmospheric Data Assimilation System, version 5.12.4 (https://giovanni.gsfc.nasa.gov/giovanni). True color images obtained from the Moderate Resolution Imaging Spectroradiometer (MODIS) on the Terra satellite were used to assess the pollution distributions visually on several selected days, and those images were downloaded from the website https://lance.modaps.eosdis.nasa.gov.

2.3 Data analysis

2.3.1 Assessment of surface transport

Hourly rBC concentrations and the corresponding wind data were used to estimate the surface transport of rBC at the Lulang site using the following formula (White et al., 1976):

$$f = \frac{1}{n}\sum_{j=1}^{n} C_j \times WS_j \times \cos\theta_j \quad (2)$$

where f is the surface transport intensity of rBC in units of μg s^{-1} m^{-2} (that is, mass transported per unit time and area); C_j and WS_j are the mean rBC concentrations (μg m^{-3}) and wind speeds (m s^{-1}) during the *j*th observation hour, respectively; θ_j is the angle between wind direction and the north-south direction during the *j*th observation hour; and n is the total number of observation hours. Generally, strong winds favor the dispersion of air pollutants for local emission sources whereas weak winds lead to accumulation. In contrast, for regional sources, strong winds can transport pollutants from upwind areas and cause high concentrations of pollutants downwind. Therefore, in this study, we viewed the surface flux intensity as a measure of the influence of regional transport in South Asia, and more specifically on the Lulang site using ground-based observations. Positive values for f were considered indicative of transport from outside the TP (e.g., the Indo-Gangetic Plain, IGP, and Bangladesh) whereas negative values indicated transport from the interior of the TP.

带格式的: 上标

删除的内容: depths

删除的内容: National Centers for Environmental Predication (NCEP, http://apps.ecmwf.int/datasets)

删除的内容: these

删除的内容: can be

删除的内容: I

删除的内容: the

删除的内容:

删除的内容: cross-boundary

2.3.2 Cluster analysis of air-mass trajectories

Three-day air mass trajectories calculated backwards in time were used to characterize the atmospheric transport of rBC to Lulang. Each trajectory was calculated for an arrival height of 150 m above ground. The trajectories were calculated hourly using the Hybrid Single-Particle Lagrangian Integrated Trajectory (HYSPLIT) model (Draxler and Rolph, 2003) developed by the Air Resource Lab (ARL) of the National Oceanic and Atmospheric Administration (NOAA). Because a large number of trajectories (887) retrieved for the entire campaign showed diverse pathways, a clustering procedure was used to establish representative pathways for the trajectories based on an angle-based distance statistics method. This was defined using the law of cosines from the following equations (Sirois and Bottenheim, 1995):

$$d_{12} = \frac{1}{n}\sum_{i=1}^{n} cos^{-1}\left(0.5 \times \frac{A_i + B_i - C_i}{\sqrt{A_i B_i}}\right) \quad (3)$$

$$A_i = (X_1(i) - X_0)^2 + (Y_1(i) - Y_0)^2 \quad (4)$$

$$B_i = (X_2(i) - X_0)^2 + (Y_2(i) - Y_0)^2 \quad (5)$$

$$C_i = (X_2(i) - X_1(i))^2 + (Y_2(i) - Y_1(i))^2 \quad (6)$$

where d_{12} is the mean angle between the two backward trajectories, which varies between 0 and π; X_0 and Y_0 represent the position of the receptor site (Lulang in the present case); X_1 (Y_1) and X_2 (Y_2) refer to backward trajectories 1 and 2, respectively. A two-step algorithm was used to produce the clusters. First, a Hartigan's K mean algorithm was used to construct several clusters of backward trajectories. Those clusters were then examined visually, and selected backward trajectories were moved from one cluster to another in order to define clusters that were easier to interpret with respect to geographical and/or anthropogenic source regions. In this study, three clusters were chosen as representative of the backward trajectory clusters. The simulation was conducted using the GIS-based TrajStat software (Wang et al., 2009).

2.3.3 Concentration-weighted trajectory (CWT) model

A CWT model was used to construct the spatial distribution of the rBC sources that potentially influenced the air sampled at Lulang. For the CWT calculations, the entire geographic region covered by the three-day backward trajectories was separated into ~8100 grid cells of 0.5° latitude × 0.5° longitude. Each grid cell was assigned a residence-time weighted concentration obtained by hourly-averaged rBC concentration associated with the trajectories that crossed that grid cell (Hsu et al., 2003):

$$C_{ij} = \frac{\sum_{l=1}^{M} c_l \tau_{ijl}}{\sum_{l=1}^{M} \tau_{ijl}} \quad (7)$$

删除的内容: backward

删除的内容: pathways

删除的内容: in

删除的内容: determine

删除的内容: (Sirois and Bottenheim, 1995)

删除的内容: n is the total number of end points in a trajectory

where C_{ij} is the average weighted-concentration in the *ij*th grid cell; C_l is the measured rBC concentration on the arrival of trajectory *l*; τ_{ijl} is the number of trajectory endpoints in the *ij*th grid cell by trajectory *l*; M is the total number of trajectories. A high C_{ij} value indicates that air parcels that travelled over the *ij*th grid cell would, on average, contribute significantly to the observed high rBC loading at Lulang.

3 Results and discussion

3.1 Characteristics of surface rBC

3.1.1 rBC loadings

A time-series plot of the hourly-averaged mass concentrations of rBC and TSP during the entire campaign is shown in Fig. 2. The hourly average mass concentrations of rBC ranged from 0.002 to 9.23 μg m^{-3} with an arithmetic mean (± standard deviation, SD) of 0.31 ± 0.55 μg m^{-3}. A frequency distribution of the rBC mass concentrations (Supplemental Fig. S5) shows that the rBC values formed a typical truncated normal distribution, with ~60% of all the data below 0.2 μg m^{-3}. However, the coefficient of variation (defined as SD/mean) for the rBC values was as high as 177%. Furthermore, ~25% of the rBC mass loadings were above the 75th percentile value of 0.33 μg m^{-3}. These results simply show that the concentrations were quite variable, and at times large loadings of rBC occur at Lulang.

The grand average mass concentration of TSP for the study was 12.65 ± 9.00 μg m^{-3}, which ranged from a minimum of 1.54 μg m^{-3} to a maximum of 73.40 μg m^{-3} (Fig. 2). The rBC particles accounted for 0.4–25.6% of TSP mass and averaged 2.6%. Supplemental Fig. S6 shows that the relationship between rBC and TSP followed two different patterns. On 21 October, the mass concentrations of rBC were highly correlated with the TSP mass concentrations (r = 0.97), but a weaker correlation (r = 0.67) was found for the other sampling days. Moreover, rBC accounted for 13.6% of TSP mass on 21 October, but the contribution was considerably smaller (2.2%) for other sampling days. As rBC is produced by combustion (Bond et al., 2013), these results indicate that combustion sources contributed significantly to TSP mass on 21 October while particles from non-combustion related sources, such as secondary aerosols and soil dust, were relatively more abundant on the other sampling days.

Fig. 1 shows the spatial distribution of BC mass concentrations at different high-altitude locations on the Himalayas and TP. Information for each study from which results were taken is summarized in Table S1. Although the sampling periods differed among the studies, BC generally exhibited larger loadings in the Himalayan foothills compared with those observed on the TP. On the other hand, the BC mass concentrations varied inversely with the altitude of the sampling sites (r = -0.81) (Fig. 1). The average rBC mass concentration at Lulang was higher than what has been measured in the interior or northern TP, but it was lower than at several locations on the southeastern TP and the Himalayan foothills (Fig. 1). The differences in BC loadings among locations can be explained by several factors. First, the concentrations are undoubtedly affected by pollutant transport

删除的内容: ing

删除的内容: S3

删除的内容: suggest

删除的内容: large loadings of rBC did

删除的内容: and TSP

删除的内容: of the TSP

删除的内容: S4

删除的内容:

删除的内容: ,

删除的内容: and i

删除的内容: attributed to

删除的内容: ;

删除的内容: f

from upwind regions (e.g., South Asia), and this is influenced by the complex topography of the area. For example, Zhang et al. (2015) found that on annual average ~50% of the BC column burden of the Himalayas and TP was due to transport from South Asia (~33% biomass and biofuel emissions and ~17% fossil fuel emissions). Second, the uncertainties caused by the inherent limitations of analytical methods themselves also help explain some of the differences in reported loadings. Indeed, previous studies have shown that the BC concentrations obtained from filter-based optical techniques (e.g., aethalometer) can be affected by the light-scattering artefacts (Virkkula et al., 2007) while laser-induced incandescence methods (e.g., SP2) can undersample small particles (Bond et al., 2013). Finally, there is still a lack of BC method intercomparisons, and there is some evidence that the differences among methods are greater for remote areas than urban ones. For instance, Wang et al. (2014) reported that a scaling factor of 2.5 was needed to adjust the eBC mass concentrations measured with an aethalometer to match SP2 measurements at a remote site on the northeastern TP while the corresponding value at an urban site was 1.3. Moreover, filter-based EC measurements based on thermal-optical reflectance methods may be affected by the presence of carbonates (Li et al., 2017). In some areas of the TP, mineral dust particles, including carbonates, can contribute considerably to the aerosol populations due to the general lack of vegetative cover and long-range transport. Therefore, limitations such as those mentioned above make it difficult to establish scaling factors to reconcile the various BC measurements on the TP to a common standard, and direct comparisons of BC data obtained by different methods can be tenuous.

3.1.2 Diurnal variations

Fig. 3 (a–c) shows the diurnal variations of the average rBC mass concentrations, PBL heights, and wind speeds during the campaign. The rBC mass concentrations decreased slightly after midnight to reach a low value of 0.16 μg m^{-3} in the early morning, around 05:00 local time (LT—all time references below are given in LT); that was followed by a sharp increase at a rate of 0.35 μg m^{-3} h^{-1} to a maximum value of 1.21 μg m^{-3} around 09:00. The rBC loadings then decreased rapidly at 0.36 μg m^{-3} h^{-1} and reached a diurnal minimum of 0.10 μg m^{-3} in the afternoon around 14:00. Thereafter, the rBC again increased gradually to a small peak of 0.26 μg m^{-3} at night around 20:00. After that, the concentrations were relatively stable until 01:00. Previous studies in urban areas have often shown a morning peak in BC caused by local rush hour traffic (e.g, Cao et al., 2009; Wang et al., 2016a). In contrast, slight morning enhancements in BC have been found at some sites on the TP, and those were attributed to local anthropogenic activities (e.g., Wang et al., 2014; Wang M. et al., 2016). In our study, a morning peak was observed at Lulang, but the rBC loadings enhancements were as much as six times the minimum values. The morning peaks were consistent with the day-to-day activities of the local residents, especially cooking, indicating that there can be some contributions of rBC from local sources. However, local emissions alone may not explain such a large concentrations increase in the morning. This can be assessed indirectly by comparing the morning peaks with the much smaller rBC enhancements in the evening around 19:00–20:00, which also were influenced by local cooking activities. Thus, the large morning peaks may have resulted from the combined effects of local activities and regional transport. As shown in Fig. 3 (a–b), the rapid morning increases in rBC were accompanied by deepening of the PBL, which suggests the possibility that regional transport had an important influence on rBC particles. Located to the southwest of Lulang, Bangladesh and the IGP are known to be strong

删除的内容: that …histransport…is influencedaffected…by the complex topography of the area. For example, Zhang et al. (2015) found that on annual average ~50% of the BC column burden of the Himalayas and TP was due to transport from South Asia (~33% by …iomass and biofuel emissions and ~17% by …ossil fuel emissions). Meanwhile, Zhao S. et al. (2017) concluded that the high altitudes of the Himalayas and TP can impede the transport of BC from the Indo-Gangetic Plain (IGP) to these regions, and therefore, the trans-Himalaya transport of BC is strongly dependent upon meteorological conditions over the IGP. …econd, the uncertainties caused by the inherent limitations of analytical methodsinstruments…themselves also help explain some of the differences the variability …n reported loadings. Indeed, previous studies have shown that the BC concentrations obtained from filter-based optical techniques (e.g., aethalometer) can beis…affected by the light …ight-scattering artifacts …rtefacts (Virkkula et al., 2007) while laser-induced incandescence methods (e.g., SP2) can undersample small particles (Bond et al., 2013). Finally, there is still a lack of BC method intercomparisons, and there is some evidence that the differences among methods aremay be…greater forin…remote areas than urban ones. For example…nstance, Wang et al. (2014) reported that a scaling factor of 2.5 was needed to adjustcorrect…the eBC mass concentrations measured with an aethalometer to match SP2 measurements at a remote site on the northeastern TP while the corresponding value at an urban site was 1.3. Moreover, filter-based BC …C measurements based on thermal-optical reflectance methods may be affected by the presence of carbonates (Li et al., 2017), …. In some areas of the TP,and…mineral dust particles, including carbonates, can contribute considerably to the aerosol populations in some areas of the TP …ue to the general lack of vegetative cover and long-range transport. ThereforeCurrently… limitations such as those mentioned above make itthere are still…difficulties…in …o ...

删除的内容: depths…eights, and wind speeds over …uring the course of the …ampaign. The rBC mass concentrations decreased slightly after midnight to reach a low value of 0.16 μg m^{-3} in the early morning, around 05:00 local time (LT—all time references below are given in LT); that was followed by a sharp increase at a rate of 0.35 μg m^{-3} h^{-1} to a maximum value of 1.21 μg m^{-3} around 09:00. The rBC loadings then decreased rapidly at a rate of ….36 μg m^{-3} h^{-1} and subsequently ...

删除的内容: /rBC…caused bylinked to…local rush hour traffic (e.g, Cao et al., 2009; Wang et al., 2016a). In contrast, slight morning enhancements in BC/rBC…have been found at some sites on the TP, and they …hose were attributed to local anthropogenic activities (e.g., Wang et al., 2014; Wang M. et al., 2016). In our study, a morning peak also …as observed at Lulang, but the rBC loadings enhancements were as large …uch as six-fold…times the over…minimum values. The morning peaks was …ere consistent with the day-to-day activities of the local residents, especially cooking, indicating that there were …an be some contributions of rBC from local sources. However, local emissions alone may not explain such a large concentrations increasedifference…in the morningconcentrations… This can be assessed indirectly by comparisons …omparing of …he morning peaks with the much smaller rBC enhancements in the evening around 19:00–20:00, which also are …ere influenced by local cooking activities. Thus, the large morning peaks may have resulted from the combined effects of local activities and regional transport. As shown in Fig. 3 (a–b), the rapid morning increases in rBC was …ere accompanied by deepening of the PBL, and therefore…hich suggests the possibility that,…regior ...

sources for BC particles (Zhang et al., 2009). The PBL height is typically shallow and stable at night, and pollutants from the IGP and Bangladesh tend to be confined near the surface at that time. After sunrise, as the PBL starts to deepen, strengthening thermals lift and eventually break up the nighttime inversion. These changes in the atmosphere provide conditions that could support the transport of pollutants to the southeastern TP.

This explanation concerning the effects of transport is further supported by the analysis of true color images of haze clouds retrieved by the MODIS on the Terra satellite (Supplemental Fig. S7). That satellite passed over the study region at ~10:30, and even though only several sampling days (20–23 October) were selected for inclusion in Fig. S7, most days exhibited similar patterns. The true color images reveal obvious pollution bands along the IGP and Bangladesh that piled up on the southern margin of the TP. The prevailing wind direction around the southeastern margin of the TP was southerly (Fig. S7), and therefore, the aerosols in the pollution bands were subject to transport along the valley of the Yarlung Tsangpo River to our sampling site. Indeed, this pathway has been considered a "leaking wall" for pollutant transport to the southeastern TP (Cao et al., 2010).

The decreasing trend in rBC loadings in the late morning at Lulang is consistent with the continued deepening of the PBL (Fig. 3b) and the strengthening winds from the northeast (see Fig. 2 and Fig. 3c). Those meteorological conditions also can explain the daily minima in the rBC loadings in the afternoon because they cause the dilution and dispersal of the ambient aerosols, including rBC. The slight enhancement of rBC at night can be attributed to shallow PBLs and low winds in addition to increased local rBC anthropogenic emissions from daily activities, such as cooking and heating. It should be noted that even though the average rBC concentration from 08:00–10:00 on 21 October was ~8 times higher than the average value for other sampling days, the diurnal pattern of 21 October was similar to that seen on other days (Fig. S8a). Indeed, the rBC diurnal loading pattern did not appear to different on this high rBC concentration day (Fig. S8 b and c). Over short time scales, such as the length of our study, one can assume that the local emission sources are relatively stable. Based on the three-day backward trajectory analysis, sudden high rBC loadings such as those on the morning on 21 October may be explained by the slow passage of air over Guwahati in northeastern India (Fig. S9). Large numbers of rBC particles likely accumulated in the air as it slowly passed over this polluted region, and it was those particles that were eventually transported to Lulang.

3.2 Meteorological effects on rBC concentrations

Wet deposition is the major mechanism by which BC aerosol is removed from the atmosphere (Bond et al., 2013). During the rain events at Lulang, the hourly precipitation varied from 0.2 to 4.0 mm (Fig. 2). The total sum of precipitation during the campaign was 104.8 mm. Rain events occurred on ~30% of the sampling period, and ~70% of the rain occurred in September due to the influx of moist warm air from the Indian and Pacific Oceans (Kang et al., 2002). The average mass concentration of rBC during rainy days (0.25 ± 0.13 μg m^{-3}) was ~45% lower than on non-rainy days (0.36 ± 0.38 μg m^{-3}). Supplemental Fig. S10 shows the impact of daily precipitation on rBC loadings; that is, the rBC mass concentrations were negatively correlated with precipitation amount (r = -0.51). In the classification scheme for daily precipitation issued by the China Meteorological Administration (GB/T 28592–2012), light, moderate, and heavy rain are defined as precipitation with ranges of 0.1–9.9, 10.0–

删除的内容: ,
删除的内容: and this can lead to
删除的内容: e preceding
删除的内容: S5
删除的内容: passes
删除的内容: S5
删除的内容: , which
删除的内容: S5
删除的内容: pollutants
删除的内容: could be
删除的内容: ed to the sampling site
删除的内容: ;
删除的内容: i
删除的内容: as
删除的内容: can be explained by
删除的内容: increased
删除的内容: speeds
删除的内容: 3
删除的内容: b and
删除的内容: ,
删除的内容: and t
删除的内容: increased
删除的内容: was
删除的内容: found to be
删除的内容: removal
删除的内容: for
删除的内容:),
删除的内容: and t
删除的内容: S6

24.9, and 25.0–49.9 mm within 24 h, respectively. When the daily precipitation was less than 10 mm, the rBC loadings had large fluctuations, ranging from 0.06 to 0.45 μg m^{-3}. However, when the daily precipitation was higher than 10 mm, the rBC values were < 0.14 μg m^{-3}, suggesting that rBC particles are removed more efficiently by moderate or strong rain compared with light rain. A *t*-test for the rBC concentrations during light and strong rains showed that there was a statistically significant difference between them at a probability for chance occurrence of $p < 0.01$.

Wind speed and wind direction play crucial roles in the dilution and dispersion of pollutants (Fast et al., 2007). Fig. 4a shows the wind speeds and directions during the study. Overall, the prevailing surface wind directions were westerly and northerly, and these sectors combined accounted for ~70% of the total wind frequencies. The average wind speed was 1.07 ± 0.93 m s^{-1}, and the higher wind speeds were most often associated northerly flow. To investigate the potential for the horizontal advection of rBC, we examined the relationships between rBC loadings and wind speed and wind direction using a bivariate polar plot (Fig. 4b). When the wind speed exceeded 1 m s^{-1}, large rBC loadings were associated with airflow from the southeast. This is the compass sector that captures transport from Yarlung Tsangpo River Valley, which as noted above can bring pollutants to our site from the IGP and Bangladesh (Cao et al., 2010; Zhao S. et al., 2017). High rBC mass concentrations also occurred under static conditions or low winds (< 1 m s^{-1}), which typically promote the accumulation of locally-generated pollutants near the Earth's surface. In contrast, low levels of rBC were observed when the winds were from the north-northwest. This is likely because upwind regions in those directions contained few rBC sources. Therefore, strong winds from the north-northwest sectors would tend to dissipate the rBC particles.

To evaluate the surface transport of rBC to Lulang from the south (arbitrarily designated as positive, from outside the TP, e.g., IGP and Bangladesh) and north (negative, from the interior of the TP), surface transport intensities were calculated from Equation (2) based on the observed rBC mass concentrations, wind speed, and wind direction at the sampling site. The estimated overall net surface transport of rBC was +0.05 ± 0.29 μg s^{-1}, indicating greater transport of rBC from outside of the TP than from the interior of it. The large coefficient of variation (580%) of the surface transport intensity reflects strong fluctuations in transport, and at least two factors likely influenced the transport processes. First, the surface fluxes were more than likely strongly affected by the prevailing winds. Fig. 5 shows the variations in the hourly-averaged surface transport intensity of rBC and the corresponding wind vectors (m s^{-1}). In general, the rBC transport intensities exhibited a clear "saw-toothed" pattern, with changes in the influx (positive) and outflux (negative) patterns corresponding to shifts in wind direction (Fig. 5a). Second, differences in the emission intensities for pollutants in the upwind areas are another factor that likely affected the transport of rBC. For example, the average influx intensity (+0.18 ± 0.27 μg s^{-1} m^{-2}) for rBC, which includes transport from IGP and Bangladesh, was two-fold stronger than the efflux intensity (-0.09 ± 0.24 μg s^{-1} m^{-2}) (Fig. 5b).

3.3 Effects of regional transport

Fig. 6a shows the three cluster-mean trajectories that were constructed from the individual three-day backward trajectories for the campaign. For discussion purposes, we arbitrarily defined a trajectory as "polluted" if it corresponded to an rBC concentration higher than the 75th percentile value of 0.33 μg m^{-3}; otherwise it was classified as "clean" trajectory. The average

删除的内容: transport
删除的内容: ,
删除的内容: and
删除的内容: .
删除的内容: possible effects of
删除的内容: ,
删除的内容: and that
删除的内容: for
删除的内容: to our site
删除的内容: ,
删除的内容: and t
删除的内容: ,
删除的内容: and t
删除的内容: speed
删除的内容: .
删除的内容: the TP
删除的内容: the
删除的内容: as noted previously, the emissions of rBC from the IGP and Bangladesh are strong, and
删除的内容: rBC
删除的内容: these areas
删除的内容: calculated

rBC mass concentrations for the three clusters and the polluted trajectories are summarized in Table 1. The air masses grouped into Cluster #1 originated from north India, and passed through central Nepal and the southern TP before arriving at Lulang. The average rBC mass concentration for Cluster #1 was 0.37 ± 0.71 μg m^{-3}. Of all 887 backward trajectories included in the analysis, ~47% were allocated to Cluster #1, and ~29% of those were considered polluted. The average rBC mass concentration for these polluted trajectories was 0.95 μg m^{-3}. The air masses grouped into Cluster #1 were responsible for many of the high rBC loadings at the receptor site. The air masses associated with Cluster #2 originated from central Bangladesh and then moved across northeastern India and to the southeast of Tibet before arriving at Lulang. The average rBC mass concentration for Cluster #2 was 0.24 ± 0.36 μg m^{-3}. The percentage of the trajectories assigned to this cluster was ~44%, and ~20% of those were regarded as polluted. The average mass concentration of the polluted trajectories in Cluster #2 was 0.75 μg m^{-3}. The air masses in Cluster #3 originated over central Tibet, and the average rBC mass concentration for this cluster (0.32 ± 0.31 μg m^{-3}) was similar to that for Cluster #1. Although the percent contribution from this cluster was ~9% of all trajectories, ~30% of the trajectories in Cluster #3 were classified as polluted, and they had a mean value of 0.72 μg m^{-3}. This implies some contributions of rBC from internal Tibetan sources.

A CWT model was used to better identify the locations of the potential source areas that provided rBC to Lulang, and a map of the CWT results for the campaign is shown in Fig. 6b. There were three main source regions contributing to the rBC pollution at Lulang. Region I was mainly composed of areas along the southern border of the Himalayan foothills, IGP, and north Bangladesh. This region had the highest CWT values, indicating that this area had the greatest probability for causing the high rBC loadings at Lulang, and it is also worth noting that there are high BC column mass densities in this area (Fig. 6c). In contrast, moderate CWT values were found for areas to the west of Lulang and adjoining regions (Region II), suggesting local anthropogenic activities in the interior of the TP also contributed to the rBC loadings at Lulang. Several cities, including Lhasa, Gongbu Jiang and Linzhi, are located ~60–350 km to the west of Lulang, and these are possible sources for anthropogenic materials. Although the population is sparse in the areas surrounding Lulang, biofuels, especially wood and yak dung, are the main energy sources for the local residents (Ping et al., 2011). Domestic heating and cooking using these fuels typically produce large quantities of rBC particles, and therefore, these sources probably affected the sampling site. Region II evidently had lesser effects on the rBC loadings compared with the Region I because the CWT values for Region II were lower. It is worth noting that even though Region III extended to the southwest of Sinkiang Province, China and several central Asian countries that emit substantial quantities of BC, this region had only minor impacts on the rBC because the air masses from Region III composed less than ~1% of the total trajectories.

3.4 Microphysical properties

3.4.1 Size distributions of rBC

Fig. S1 shows that rBC core size distribution was well represented by a mono-modal lognormal fit. This is consistent with the size distributions constructed from previous SP2-based observations made across the globe, including urban, rural, and remote

删除的内容: the air masses grouped into this cluster
删除的内容: ,
删除的内容: and t
删除的内容: %;
删除的内容: ;
删除的内容: and t
删除的内容: .
删除的内容: T
删除的内容: ;
删除的内容: this
删除的内容: .
删除的内容: Fig. 6b shows
删除的内容: ,
删除的内容: and t
删除的内容: these
删除的内容: s
删除的内容: transporting
删除的内容: to
删除的内容: . Further evidence of this can be seen in the map of average
删除的内容: the TP and South Asia during the sampling period
删除的内容: —it confirms large BC loadings along the southern border of Himalayan foothills, IGP, and Bangladesh, and this is consistent with the large CWT values in Region I discussed above. Although the high altitude of the Himalayas can inhibit air flow from Region I to the TP, previous studies indicate that pollutants can be ...
删除的内容: in
删除的内容: presumptive
删除的内容: Thus, air masses that arrived at Lulang from the wes ...
删除的内容: (e.g.,
删除的内容:)
删除的内容: Emissions from
删除的内容: contain
删除的内容: hence
删除的内容: domestic
删除的内容: affects
删除的内容: 's
删除的内容: although
删除的内容: ,
删除的内容: source
删除的内容: ,
删除的内容: which

areas (e.g., Schwarz et al., 2008; Liu et al., 2010; McMeeking et al., 2011; Huang et al., 2012; Wang et al., 2014). As shown in Fig. 2, the hourly-averaged mass median diameters (MMD—the VED at the peak of the mass distribution) varied broadly from 98 to 255 nm during the study, and the average was 160 ± 23 nm. The rBC MMDs exhibited diurnal patterns similar to the rBC mass concentrations; that is, they peaked in the morning around 09:00 (~183 nm), fell to a minimum in the afternoon around 14:00 (~147 nm), then rose again in the evening, and finally stabilized at night (~163 nm) (Fig. 3d).

Although size-segregated filter-based measurements made with cascade impactors provide information on the aerodynamic diameters of BC particles, they measure both the BC cores and any coatings on the particles. In contrast, the SP2 measures the rBC core size alone. Consequently, we only compared our results with SP2 observations made in previous studies. Because of the different rBC densities assumed in the various studies, we normalized them to the same density of 1.8 g cm^{-3} to facilitate direct comparisons. The average rBC MMD at Lulang fell into the lower range reported in previous SP2 studies (~155–240 nm; Huang et al., 2012, and references therein), and it was lower than some results reported for remote areas, such as 181 nm at Qinghai Lake, northeastern TP (Wang et al., 2014), 194 nm at the Pallas Global Atmosphere Watch station, Finnish Arctic (Raatikainen et al., 2015), and 220–240 at the high alpine research station Jungfraujoch, Switzerland (Liu et al., 2010).

The variations in rBC MMDs among sites were likely related to the following factors. First, the various emission sources produce rBC particles of different sizes. For example, Sahu et al. (2012) observed larger average rBC MMD in biomass burning plumes (193 nm) compared with fossil fuel plumes (175 nm). Wang et al. (2016b) reported a higher average rBC MMD for coal burning (215 nm) compared with particles from a traffic source (189 nm). Second, transport histories matter because aging of the particles can affect the size distributions of rBC. Take the cluster analysis as an example: the average rBC MMD was the largest (184 ± 17 nm) when the polluted air masses originated from central Bangladesh (Cluster #2). In contrast, smaller rBC MMDs were found when the polluted air masses came from North India (Cluster #1, 173 ± 26 nm) or the central TP (Cluster #3, 177 ± 19 nm). These air masses originated from different sources regions, and they may have had different rBC sizes initially; but the rBC core sizes also may have changed during transport through coagulation. It should be noted that a *t*-test for the rBC MMDs from different clusters showed that there was a statistically significant difference between Cluster #1 and #2 ($p < 0.01$), but was not significant between Cluster #2 and #3 ($p = 0.09$).

Finally, wet deposition may exert a significant effect on the rBC size distributions. This can be seen in Fig. 7 which presents a comparison of the frequency distributions of rBC MMDs during rainy and non-rainy sampling days. The rBC MMDs varied from 112 to 255 nm with an average of 164 ± 21 nm for the non-rainy days, and about 50% of the MMDs were within the range of 150–175 nm. In contrast, the rBC MMDs for rainy days shifted toward smaller sizes, varying from 98 to 230 nm and averaging 145 ± 25 nm. About 40% of the MMDs for the rainy day samples were in the range of 125–145 nm. We note that the sizes of the particles on rainy days may be representative of local sources because rain also fell over South Asia, and therefore, there was little long-range transport of rBC to Lulang under those conditions. Compared with non-rainy days, the smaller rBC on rainy days can be explained by the absence of long-range transport and by the preferential wet scavenging of larger rBC cores (Taylor et al., 2014).

删除的内容: of these

删除的内容: Although t

删除的内容: different

删除的内容: are

删除的内容: than that in

删除的内容:),

删除的内容: and

删除的内容: air mass

删除的内容: affect

删除的内容: Moreover, more aged particles in the plumes tend to be larger than fresher particles from close to the source (Moteki et al., 2007)

删除的内容: impact

删除的内容: ~

删除的内容: T

删除的内容: long

删除的内容: the

删除的内容: size

删除的内容: reduced atmospheric lifetimes for large rBC particles due to

3.4.2 Evolution of rBC mixing state

The average F_{rBC} was 39 ± 8% (range of 20–68%, Fig. 2) during the entire campaign, which is lower than what has been reported for Qinghai Lake (59%, Wang et al., 2015a) where a similar method was used to measure the internal mixing of rBC. Air masses in Cluster #2 showed the highest internal mixing of rBC particles (40%), followed by Cluster # 1 (38%), and Cluster #3 (34%). The low percentages of internal mixing for rBC particles in these three clusters indicates a relatively low level of particle aging. This implies that freshly-emitted local rBC particles were part of the sample population. Fig. 8a shows that the diurnal cycle of F_{rBC} at Lulang typically exhibited "two peaks and two valleys". The percentage of internally-mixed rBC reached a peak value of 45% in the morning around 07:00–08:00, followed by a decreasing trend to a low value of 35% around 10:00. The internally-mixed rBC then increased to a secondary peak value of 44% in the afternoon around 14:00, and again slowly decreased to a minimum of 33% around 01:00.

The variations in percentages of internally-mixed rBC in the morning further provide evidence for the combined effects of local activities and regional transport on the rBC aerosol. That is, the enhancement of internally-mixed rBC around 07:00–08:00 can be attributed to rBC aging, which indicates impacts from regional transport. The decreasing trend of F_{rBC} around 09:00–10:00 was likely due to an increase in fresh rBC particles emitted by local anthropogenic activities even though the local population was small. As the day progressed, from 10:00 to 19:00, F_{rBC} varied with O_3 mixing ratios (Fig. 8a), suggesting a possible effect of oxidants on the internal mixing of rBC. It can be seen in Fig. 8b that F_{rBC} was positively correlated with the O_3 mixing ratios (r = 0.89), indicating that more internal mixing for rBC particles occurred under more oxidizing conditions. Further, the observed increasing trend for internally-mixed rBC from 10:00–14:00 can be explained by the mixing of rBC particles with secondary aerosols (e.g., non-refractory inorganic and organic compounds) that resulted from enhanced photochemical oxidation due to the daily cycle in insolation.

To further investigate the effects of photochemical oxidation on the rBC mixing state, we compared the diurnal variations of internal mixing for rBC particles at Lulang with observations made at Qinghai Lake, a site in the northeastern TP where studies were conducted in October 2011 (Fig. 8c). The rBC and O_3 at Qinghai Lake were measured with the same type of SP2 as in this study and an ultraviolet photometer, respectively. Detailed descriptions of the Qinghai Lake study may be found in Wang et al., 2014; 2015b. As shown in Fig. 8c, only one F_{rBC} peak was observed at Qinghai Lake in the afternoon between 12:00–17:00, which was different from what we observed at Lulang. This difference can be explained by the fact that rBC in the early morning at Qinghai Lake was not affected by long-range transport owing to the topography of the region (Wang et al., 2014). Even so, similar to Lulang, the F_{rBC} during the daytime (08:00–18:00) at Qinghai Lake was positively correlated with the O_3 mixing ratio (r = 0.75, Fig. 8d), and these results are additional evidence that photochemical oxidation is involved in the formation the coatings on rBC particles from the TP. Moreover, the variations in F_{rBC} during the daytime at Lulang also covaried with the PBL heights, indicating that aged rBC particles may have been transported from aloft to the surface.

删除的内容: hourly-averaged

删除的内容: ranged from 20 to 68% (average =

删除的内容: and that

删除的内容: ,

删除的内容: and t

删除的内容: may have been

删除的内容: value

删除的内容: of

删除的内容: such as cooking

删除的内容: ,

删除的内容: between

删除的内容: and

删除的内容: To further investigate the impact of oxidant levels on the internal mixing of rBC, the F_{rBC} collected between 10:00–19:00 was plotted against the O_3 mixing ratios.

删除的内容: with the rBC particles due to

删除的内容: As shown in Fig. 8b, the slope of F_{rBC} versus O_3 during midday was 0.44 % ppb^{-1}, and this reflects the rate at which oxidation affects rBC mixing. In contrast, the decrease in F_{rBC} from 15:00–20:00 can be ascribed to the small impacts from secondary aerosols due to less oxidizing conditions.

删除的内容: and

删除的内容: ,

删除的内容: and d

删除的内容: and that

删除的内容: However, at Qinghai Lake, the slope of the F_{rBC} versus O_3 was 0.24% ppb^{-1} from 08:00–16:00, and therefore, the rate at which the internally-mixed rBC increased with O_3 was lower than at Lulang by a factor of ~2. The more rapid increase in O_3 at Lulang (4.8 ppb h^{-1}) compared with Qinghai Lake (3.2 ppb h^{-1}) shows that the oxidation rates leading to the formation of internally mixed rBC at Qinghai Lake were lower than at Lulang even though O_3 was higher at Qinghai Lake (58.7 ppb) than that at Lulang (32.1 ppb). Similar results have been found in urban areas of Beijing and Xi'an, China (Wang et al., 2017), and the relevant conclusion from that study was that photochemical oxidation can be important for formation the coatings on rBC particles.

3.5 rBC optical properties

The average b_{abs} at λ = 870 nm for the campaign was 2.9 ± 2.4 Mm^{-1} (Fig. 2). Some organic materials (also called brown carbon) can cause significant light absorption, but those effects are mainly at short wavelengths (e.g., λ = 370 nm), and they have nearly no absorption in the near-infrared spectral region (e.g., λ = 870 nm) (Laskin et al., 2015). Consequently, it is reasonable to calculate the mass absorption cross section of rBC (MAC_{rBC}, m^2 g^{-1}), which describes the degree of light absorption per-unit-mass of rBC, by dividing the b_{abs} measured with the PAX_{870} by the mass concentration of rBC detected with the SP2 (MAC_{rBC} = b_{abs}/rBC). Fig. 9 shows that the MAC_{rBC} frequency distributions were mono-modal lognormal for all samples from the campaign and for the data stratified by the three trajectory clusters. The peak in the frequency MAC_{rBC} distribution for the entire campaign was 7.6 m^2 g^{-1}, and there were slightly higher values for Cluster #1 (8.0 m^2 g^{-1}) and Cluster #2 (7.8 m^2 g^{-1}) compared with Cluster #3 (7.5 m^2 g^{-1}).

Absorption enhancements for the rBC (E_{abs} = MAC_{rBC}/$MAC_{rBC,uncoated}$) were calculated to further characterize the rBC particles' optical properties. As the SP2 only determines the rBC core size, the hourly-averaged MMDs for the rBC were input into the Mie model to calculate the MAC_{rBC} of uncoated rBC particles ($MAC_{rBC,uncoated}$), assuming that the uncoated rBC particles were spherical and homogeneous. A more detailed description of the Mie algorithms may be found in Bohren and Huffman (2008). For these calculations, the refractive index of 1.85-0.71*i* at λ = 550 nm suggested by Bond and Bergstrom (2006) was first used in the Mie model to estimate the $MAC_{rBC,uncoated}$. Those values were then converted to the $MAC_{rBC,uncoated}$ at λ = 870 nm based on an rBC absorption Ångström exponent of 1.0 (Moosmüller et al., 2011). Finally, the average rBC absorption enhancement was calculated by comparing the MAC_{rBC} at λ = 870 nm for rBC with and without coatings. As shown in Fig. 9, there were several anomalously large MAC_{rBC} values that were likely caused by the uncertainties associated with extremely low b_{abs} and rBC mass concentrations. To avoid spurious results such as these, only MAC_{rBC} values in the lower 90th percentile of all data were used to calculate the E_{abs}. As shown in Supplemental Fig. S11, the E_{abs} values generally followed a mono-modal lognormal distribution with a peak value of 1.9, which is an indication that the light absorption of coated rBC particles was significantly greater than that of uncoated ones.

To investigate the potential impacts of rBC size and mixing state on light absorption, the E_{abs} values were plotted against the F_{rBC} values and MMDs (Fig. 10). As shown in Fig. 10a, the E_{abs} was strongly positive correlated with the F_{rBC} (r = 0.96), and this supports our conclusion that there was an enhancement of light absorption by internally-mixed—that is, coated—rBC particles. The slope of the regression line was 0.03 $\%^{-1}$, which may be considered a rough estimate of the effects of the coatings on light absorption. This means that if the fraction of thickly-coated rBC particles increased by one percent, the rBC particles would absorb 3% more light. If the results of the linear regression shown in Fig. 10a are extrapolated to a condition in which rBC is completely uncoated (that is, F_{rBC} or x = 0%), the E_{abs} would be 1.1, which is close to the theoretical value of 1.0 for uncoated rBC. At the other extreme, if all rBC particles were internally mixed (F_{rBC} or x = 100%), the E_{abs} would be as high as 4.4, which appears physically implausible. This result is confined to a narrow range of conditions, however, that is, small rBC core diameters with the thick coatings (Bond et al., 2006). Moreover, it is noteworthy that several studies have shown

删除的内容: Hourly-averaged
删除的内容: measured with the PAX_{870} varied from 0.1–22.2 Mm^{-1} with a grand average for the study of 2.1 ± 2.0
删除的内容: only in the
删除的内容: can be calculated
删除的内容: all were mono-modal and lognormals
删除的内容: 7.0
删除的内容: 7.2
删除的内容: 7.4
删除的内容: 6.7
删除的内容: T
删除的内容: absorption enhancements
删除的内容: investigate
删除的内容: with the assumption
删除的内容: extremely
删除的内容: anomalous
删除的内容: due to
删除的内容: than the
删除的内容: S7
删除的内容: 1.8
删除的内容: by
删除的内容: by
删除的内容: and this
删除的内容: internally-mixed
删除的内容: 4.3

non-linear relationships between E_{abs} and the internal mixing of rBC (e.g., Zhang et al., 2016; Liu et al., 2015). In those cases, the E_{abs} tended to be stable over a large range of coating thicknesses. If that were the case in our study, the E_{abs} would be lower than the calculated value of 4.4.

As shown in Fig. 10b, the E_{abs} was non-linearly related to the MMDs of the rBC. When rBC MMD < 170 nm, the E_{abs} varied inversely with rBC core size, indicating that smaller rBC particles potentially have a stronger ability to amplify light absorption than large ones. This can be explained by the greater tendency of small rBC particles to form coatings than the large ones, which is due to the well-known relationship between particle surface area and volume (see the positive correlation between F_{rBC} and MMDs in Supplemental Fig. S12). The variations in E_{abs} were relatively constant for rBC MMD > 170 nm. When coatings form by condensation, a 1/diameter dependence would apply to the condensation rate. Thus, larger rBC cores have smaller degree of internal mixing and weaker absorption amplification than smaller cores on the one hand, but on the other hand, larger rBC core size also would decrease the $MAC_{rBC,uncoated}$ according to the Mie model (see the relationship between $MAC_{rBC,uncoated}$ and MMD in Fig. S12). Eventually, the decrease in light absorbing ability for the measured ambient rBC (that is, the MAC_{rBC}) and for the assumed uncoated rBC particles (that is, $MAC_{rBC,uncoated}$) would cancel out causing a constant value for E_{abs}. Indeed, Bond et al. (2006) reported that the amplification was nearly constant for rBC cores > ~150 nm.

4 Conclusions

The mass concentrations, size distributions, mixing state, and optical properties of rBC aerosol were studied at Lulang on the southeastern TP, China. The mass concentration of rBC, averaged over the entire campaign, was 0.31 ± 0.55 μg m^{-3}, and the rBC particles accounted for 2.6% of TSP mass. A clear diurnal pattern in rBC mass concentrations was observed: high values occurred in the early morning due to the combined effects of local anthropogenic activities and regional transport while low values in the afternoon were ascribed to the dispersion of the rBC due to deepening of the PBL and higher wind speeds. The relationship observed between rainfall and rBC indicated that rBC particles were more efficiently removed by moderate and heavy precipitation (>10 mm) than by light rain. A bivariate polar plot showed that high rBC loadings were associated with strong winds from the southeast or static wind conditions. The estimated overall net surface transport intensity of rBC was +0.05 ± 0.29 μg s^{-1} m^{-2}. Those calculations showed that more rBC was brought to the site from outside the TP than from the interior of the TP. Moreover, air mass trajectory clusters and a concentration-weighted trajectory model indicated that sources in north India were the most important influences on rBC at Lulang, but local contributions were not negligible.

The rBC VEDs showed approximately mono-modal lognormal distributions. The hourly-average rBC MMD was 160 ± 23 nm, and the MMDs varied among air parcels. The MMDs shifted toward smaller sizes (145 nm) on rainy days compared with non-rainy days (164 nm). The average F_{rBC} for the study was 39 ± 8%, suggesting uncoated or thinly-coated rBC particles composed the bulk of the rBC population. Two peaks in F_{rBC} were observed: one was in the morning, which was attributed to atmospheric aging processes; the other was in the afternoon, which was explained by enhancements caused by photochemical oxidation and the mixing aged rBC particles from aloft into the surface. A strong correlation between F_{rBC} and O_3 was found during the

删除的内容: , and
删除的内容: i
删除的内容: is
删除的内容: should
删除的内容: 4.3
删除的内容: correlated negatively
删除的内容: the
删除的内容: small rBC particles
删除的内容: (see the positive correlation between F_{rBC} and MMDs in Supplemental Fig. S8)
删除的内容: This is because that
删除的内容: .
删除的内容: B
删除的内容: calculated by
删除的内容: 8
删除的内容: both the
删除的内容: similarly
删除的内容: those
删除的内容: dissipation
删除的内容: are
删除的内容: ,
删除的内容: and t
删除的内容: d
删除的内容: particle sizes
删除的内容: different
删除的内容: the
删除的内容: aerosol
删除的内容: and that
删除的内容: and that

daytime at Lulang (10:00–19:00), indicating that the photochemical oxidation played an important role in the internal mixing of rBC with other materials. A similar relationship was found for samples from near Qinghai Lake in the northeastern TP. The grand average b_{abs} (at $\lambda = 870$ nm) for the study was 2.9 ± 2.4 Mm^{-1}. The MAC_{rBC} values showed a mono-modal lognormal distribution with a peak value of 7.6 $m^2 g^{-1}$. Slightly higher MAC_{rBC} values were found for air masses from North India (8.0 $m^2 g^{-1}$) and central Bangladesh (7.8 $m^2 g^{-1}$) compared with air transported from central Tibet (7.5 $m^2 g^{-1}$). By dividing the observed MAC_{rBC} measured with the SP2 and PAX_{870} by the $MAC_{rBC,uncoated}$ calculated from the Mie model, the average E_{abs} was estimated to be 1.9. This suggests that the light absorption by coated rBC particles was significantly amplified compared with uncoated ones. Furthermore, the E_{abs} was positively correlated with F_{rBC}, indicating an enhancement of light absorption by internally-mixed rBC particles. The E_{abs} showed a negative correlation with the rBC MMDs for the particle cores < 170 nm, but it was nearly constant for larger rBC cores. We should note that the sources, transport, and radiative effects of the rBC as well as atmospheric conditions likely vary in complex ways with season, and therefore the results from our study (in autumn) are not necessarily representative of other times of the year. Indeed, additional studies need to be conducted to determine how the rBC aerosol at our site and others changes with season.

删除的内容: plays

删除的内容: , but regression analyses showed that the rate of increase in F_{rBC} with O_3 was greater at Lulang than at Qinghai Lake (0.44 versus 0.24% ppb^{-1}). These results suggest that the rBC particles in Lulang formed internal mixtures more rapidly than those at Qinghai Lake

删除的内容: Hourly-averaged

删除的内容: varied from 0.1–22.2 Mm^{-1} over the study with an overall average of 2.1 ± 2.0

删除的内容: , and

删除的内容: 7.0

删除的内容: 7.2

删除的内容: 7.4

删除的内容: 6.7

删除的内容: 1.8

删除的内容: ,

删除的内容: ing

删除的内容: the

Acknowledgments

This work was supported by the National Natural Science Foundation of China (41230641, 41503118, 41625015, and 41661144020). The authors are grateful to the Integrated Observation and Research Station for Alpine Environment in South-East Tibet, Chinese Academy of Sciences, for their assistance with field sampling.

References

Babu, S. S., Chaubey, J. P., Moorthy, K. K., Gogoi, M. M., Kompalli, S. K., Sreekanth, V., Bagare, S. P., Bhatt, B. C., Gaur, V. K., Prabhu, T. P., and Singh, N. S.: High altitude (similar to 4520 m amsl) measurements of black carbon aerosols over western trans-Himalayas: Seasonal heterogeneity and source apportionment, J. Geophys. Res., 116, D24201, doi:10.1029/2011JD016722, 2011.

Bohren, C. F., and Huffman, D. R.: Absorption and scattering of light by small particles, John Wiley & Sons, 2008.

Bond, T. C., and Bergstrom, R. W.: Light absorption by carbonaceous particles: an investigative review, Aerosol Sci. Technol., 40, 27–67, doi:10.1080/02786820500421521, 2006.

Bond, T. C., Habib, G., and Bergstrom, R. W.: Limitations in the enhancement of visible light absorption due to mixing state, J. Geophys. Res., 111, D20211, doi:10.1029/2006JD007315, 2006.

Bond, T. C., Doherty, S. J., Fahey, D. W., Forster, P. M., Berntsen, T., DeAngelo, B. J., Flanner, M. G., Ghan, S., Karcher, B., Koch, D., Kinne, S., Kondo, Y., Quinn, P. K., Sarofim, M. C., Schultz, M. G., Schulz, M., Venkataraman, C., Zhang, H., Zhang, S., Bellouin, N., Guttikunda, S. K., Hopke, P. K., Jacobson, M. Z., Kaiser, J. W., Klimont, Z., Lohmann, U.,

Schwarz, J. P., Shindell, D., Storelvmo, T., Warren, S. G., and Zender, C. S.: Bounding the role of black carbon in the climate system: A scientific assessment, J. Geophys. Res. Atmos., 118, 5380–5552, doi:10.1002/jgrd.50171, 2013.

Cao, J.-J., Zhu, C.-S., Chow, J. C., Watson, J. G., Han, Y.-M., Wang, G.-h., Shen, Z.-x., and An, Z.-S.: Black carbon relationships with emissions and meteorology in Xi'an, China, Atmos. Res., 94, 194–202, doi:10.1016/j.atmosres.2009.05.009, 2009.

Cao, J.: The importance of aerosols in the earth system: science and engineering perspectives, Aerosol Sci. Eng., 1, 1–6, doi:10.1007/s41810-017-0005-1, 2017.

Cao, J. J., Tie, X. X., Xu, B. Q., Zhao, Z. Z., Zhu, C. S., Li, G. H., and Liu, S. X.: Measuring and modeling black carbon (BC) contamination in the SE Tibetan Plateau, J. Atmos. Chem., 67, 45–60, doi:10.1007/s10874-011-9202-5, 2010.

Chen, P., Kang, S., Bai, J., Sillanpää, M., and Li, C.: Yak dung combustion aerosols in the Tibetan Plateau: Chemical characteristics and influence on the local atmospheric environment, Atmos. Res., 156, 58–66, 2015.

Cong, Z., Kang, S., Kawamura, K., Liu, B., Wan, X., Wang, Z., Gao, S., and Fu, P.: Carbonaceous aerosols on the south edge of the Tibetan Plateau: concentrations, seasonality and sources, Atmos. Chem. Phys., 15, 1573–1584, doi:10.5194/acp-15-1573-2015, 2015.

Draxler, R. R. and Rolph, G. D.: HYSPLIT (HYbrid Single-Particle Lagrangian Integrated Trajectory) Model access via NOAA ARL READY Website. http://www.arl.noaa.gov/ready/hysplit4.htmlNOAA Air Resources Laboratory, Silver Spring, MD., 2003.

Dyurgerov, M. B., and Meier, M. F.: Twentieth century climate change: Evidence from small glaciers, Proc. Natl. Acad. Sci. U. S. A., 97, 1406–1411, doi:10.1073/pnas.97.4.1406, 2000.

Engling, G., Zhang, Y.-N., Chan, C.-Y., Sang, X.-F., Lin, M., Ho, K.-F., Li, Y.-S., Lin, C.-Y., and Lee, J. J.: Characterization and sources of aerosol particles over the southeastern Tibetan Plateau during the Southeast Asia biomass-burning season, Tellus Ser. B-Chem. Phys. Meteorol., 63, 117–128, doi:10.1111/j.1600-0889.2010.00512.x, 2011.

Fast, J. D., de Foy, B., Acevedo Rosas, F., Caetano, E., Carmichael, G., Emmons, L., McKenna, D., Mena, M., Skamarock, W., Tie, X., Coulter, R. L., Barnard, J. C., Wiedinmyer, C., and Madronich, S.: A meteorological overview of the MILAGRO field campaigns, Atmos. Chem. Phys., 7, 2233–2257, https://doi.org/10.5194/acp-7-2233-2007, 2007.

Gysel, M., Laborde, M., Olfert, J. S., Subramanian, R., and Grohn, A. J.: Effective density of Aquadag and fullerene soot black carbon reference materials used for SP2 calibration, Atmos. Meas. Tech., 4, 2851–2858, doi:10.5194/amt-4-2851-2011, 2011.

He, C., Li, Q., Liou, K.-N., Takano, Y., Gu, Y., Qi, L., Mao, Y., and Leung, L. R.: Black carbon radiative forcing over the Tibetan Plateau, Geophys. Res. Lett., 41, 7806–7813, doi:10.1002/2014GL062191, 2014.

Hsu, Y.-K., Holsen, T. M., and Hopke, P. K.: Comparison of hybrid receptor models to locate PCB sources in Chicago, Atmos. Environ., 37, 545–562, https://doi.org/10.1016/S1352-2310(02)00886-5, 2003.

Huang, X. F., Sun, T. L., Zeng, L. W., Yu, G. H., and Luan, S. J.: Black carbon aerosol characterization in a coastal city in South China using a single particle soot photometer, Atmos. Environ., 51, 21–28, https://doi.org/10.1016/j.atmosenv.2012.01.056, 2012.

Huintjes, E., Loibl, D., Lehmkuhl, F., and Schneider, C.: A modelling approach to reconstruct Little Ice Age climate from remote-sensing glacier observations in southeastern Tibet, Ann. Glaciol., 57, 359–370, https://doi.org/10.3189/2016AoG71A025, 2016.

Immerzeel, W. W., van Beek, L. P. H., and Bierkens, M. F. P.: Climate change will affect the Asian water towers, Science, 328, 1382–1385, doi:10.1126/science.1183188, 2010.

Jacobson, M. Z.: Strong radiative heating due to the mixing state of black carbon in atmospheric aerosols, Nature, 409, 695–697, doi:10.1038/35055518, 2001.

Kang, S., Mayewski, P. A., Qin, D., Yan, Y., Zhang, D., Hou, S., and Ren, J.: Twentieth century increase of atmospheric ammonia recorded in Mount Everest ice core, J. Geophys. Res., 107(D20), 4595, doi:10.1029/2001JD001413, 2002.

Kang, S., Wang, F., Morgenstern, U., Zhang, Y., Grigholm, B., Kaspari, S., Schwikowski, M., Ren, J., Yao, T., Qin, D., and Mayewski, P. A.: Dramatic loss of glacier accumulation area on the Tibetan Plateau revealed by ice core tritium and mercury records, The Cryosphere, 9, 1213-1222, 2015.

Ke, L., Ding, X., Li, W., and Qiu, B.: Remote sensing of glacier change in the central Qinghai-Tibet Plateau and the relationship with changing climate, Remote Sens, 9, 114, doi:10.3390/rs9020114, 2017.

Laskin, A., Laskin, J., and Nizkorodov, S. A.: Chemistry of atmospheric brown carbon, Chem. Rev., 115, 4335–4382, doi:10.1021/cr5006167, 2015.

Laborde, M., Mertes, P., Zieger, P., Dommen, J., Baltensperger, U., and Gysel, M.: Sensitivity of the Single Particle Soot Photometer to different black carbon types, Atmos. Meas. Tech., 5, 1031-1043, doi:10.5194/amt-5-1031-2012, 2012.

Lau, K. M. and Kim, K. M.: Observational relationships between aerosol and Asian monsoon rainfall, and circulation, Geophys. Res. Lett., 33, L21810, doi:10.1029/2006GL027546, 2006.

Li, C., Bosch, C., Kang, S., Andersson, A., Chen, P., Zhang, Q., Cong, Z., Chen, B., Qin, D., and Gustafsson, Ö.: Sources of black carbon to the Himalayan–Tibetan Plateau glaciers, Nature Communications, 7, 12574, 10.1038/ncomms12574, 2016a.

Li, C., Yan, F., Kang, S., Chen, P., Hu, Z., Gao, S., Qu, B., and Sillanpää, M.: Light absorption characteristics of carbonaceous aerosols in two remote stations of the southern fringe of the Tibetan Plateau, China, Atmos. Environ., 143, 79–85, 2016b.

Li, C., Chen, P., Kang, S., Yan, F., Hu, Z., Qu, B., and Sillanpää, M.: Concentrations and light absorption characteristics of carbonaceous aerosol in $PM_{2.5}$ and PM_{10} of Lhasa city, the Tibetan Plateau, Atmos. Environ., 127, 340–346, 2016c.

Li, C., Yan, F., Kang, S., Chen, P., Han, X., Hu, Z., Zhang, G., Hong, Y., Gao, S., Qu, B., Zhu, Z., Li, J., Chen, B., and Sillanpää, M.: Re-evaluating black carbon in the Himalayas and the Tibetan Plateau: concentrations and deposition, Atmos. Chem. Phys., 17, 11899–11912, 2017.

Liu, D., Flynn, M., Gysel, M., Targino, A., Crawford, I., Bower, K., Choularton, T., Juranyi, Z., Steinbacher, M., Hueglin, C., Curtius, J., Kampus, M., Petzold, A., Weingartner, E., Baltensperger, U., and Coe, H.: Single particle characterization of black carbon aerosols at a tropospheric alpine site in Switzerland, Atmos. Chem. Phys., 10, 7389–7407, doi:10.5194/acp-10-7389-2010, 2010.

Liu, S., Aiken, A. C., Gorkowski, K., Dubey, M. K., Cappa, C. D., Williams, L. R., Herndon, S. C., Massoli, P., Fortner, E. C., Chhabra, P. S., Brooks, W. A., Onasch, T. B., Jayne, J. T., Worsnop, D. R., China, S., Sharma, N., Mazzoleni, C., Xu, L., Ng, N. L., Liu, D., Allan, J. D., Lee, J. D., Fleming, Z. L., Mohr, C., Zotter, P., Szidat, S., and Prevot, A. S. H.: Enhanced light absorption by mixed source black and brown carbon particles in UK winter, Nat. Commun., 6, 8435, doi:10.1038/ncomms9435, 2015.

Loibl, D., Lehmkuhl, F., and Grießinger, J.: Reconstructing glacier retreat since the Little Ice Age in SE Tibet by glacier mapping and equilibrium line altitude calculation, Geomorphology, 214, 22–39, http://dx.doi.org/10.1016/j.geomorph.2014.03.018, 2014.

Lu, Z., Streets, D. G., Zhang, Q., and Wang, S.: A novel back-trajectory analysis of the origin of black carbon transported to the Himalayas and Tibetan Plateau during 1996–2010, Geophys. Res. Lett., 39, L01809, 10.1029/2011GL049903, 2012.

Ma, J. Z., Tang, J., Li, S. M., and Jacobson, M. Z.: Size distributions of ionic aerosols measured at Waliguan Observatory: Implication for nitrate gas-to-particle transfer processes in the free troposphere, J. Geophys. Res., 108(D17), 4541, doi:10.1029/2002JD003356, 2003.

Marinoni, A., Cristofanelli, P., Laj, P., Duchi, R., Calzolari, F., Decesari, S., Sellegri, K., Vuillermoz, E., Verza, G. P., Villani, P., and Bonasoni, P.: Aerosol mass and black carbon concentrations, a two year record at NCO-P (5079 m, Southern Himalayas), Atmos. Chem. Phys., 10, 8551–8562, doi:10.5194/acp-10-8551-2010, 2010.

McMeeking, G. R., Morgan, W. T., Flynn, M., Highwood, E. J., Turnbull, K., Haywood, J., and Coe, H.: Black carbon aerosol mixing state, organic aerosols and aerosol optical properties over the United Kingdom, Atmos. Chem. Phys., 11, 9037–9052, doi:10.5194/acp-11-9037-2011, 2011.

Moosmüller, H., Chakrabarty, R. K., Ehlers, K. M., and Arnott, W. P.: Absorption Ångström coefficient, brown carbon, and aerosols: basic concepts, bulk matter, and spherical particles, Atmos. Chem. Phys., 11, 1217–1225, 10.5194/acp-11-1217-2011, 2011.

Pant, P., Hegde, P., Dumka, U. C., Sagar, R., Satheesh, S. K., Moorthy, K. K., Saha, A., and Srivastava, M. K.: Aerosol characteristics at a high-altitude location in central Himalayas: Optical properties and radiative forcing, J. Geophys. Res., 111, D17206, doi:10.1029/2005JD006768, 2006.

Peng, J. F., Hu, M., Guo, S., Du, Z. F., Zheng, J., Shang, D. J., Zamora, M. L., Zeng, L. M., Shao, M., Wu, Y. S., Zheng, J., Wang, Y., Glen, C. R., Collins, D. R., Molina, M. J., and Zhang, R. Y.: Markedly enhanced absorption and direct radiative forcing of black carbon under polluted urban environments, Proc. Natl. Acad. Sci. U. S. A., 113, 4266–4271, doi:10.1073/pnas.1602310113, 2016.

删除的内容: Li, Z., Tian, L., Wu, H., Wang, W., Zhang, S., Zhang, J., and Li, X.: Changes in glacier extent and surface elevations in the Depuchangdake region of northwestern Tibet, China, Quat. Res., 85, 25–33, https://doi.org/10.1016/j.yqres.2015.12.005, 2016.

删除的内容: Moteki, N., Kondo, Y., Miyazaki, Y., Takegawa, N., Komazaki, Y., Kurata, G., Shirai, T., Blake, D. R., Miyakawa, T., and Koike, M.: Evolution of mixing state of black carbon particles: Aircraft measurements over the western Pacific in March 2004, Geophys. Res. Lett., 34, L11803, doi:10.1029/2006GL028943, 2007.

Petzold, A., Ogren, J. A., Fiebig, M., Laj, P., Li, S. M., Baltensperger, U., Holzer-Popp, T., Kinne, S., Pappalardo, G., Sugimoto, N., Wehrli, C., Wiedensohler, A., and Zhang, X. Y.: Recommendations for reporting "black carbon" measurements, Atmos. Chem. Phys., 13, 8365–8379, 2013.

Ping, X., Jiang, Z., and Li, C.: Status and future perspectives of energy consumption and its ecological impacts in the Qinghai–Tibet region, Renew. Sust. Energ. Rev., 15, 514–523, https://doi.org/10.1016/j.rser.2010.07.037, 2011.

Raatikainen, T., Brus, D., Hyvärinen, A. P., Svensson, J., Asmi, E., and Lihavainen, H.: Black carbon concentrations and mixing state in the Finnish Arctic, Atmos. Chem. Phys., 15, 10057–10070, doi:10.5194/acp-15-10057-2015, 2015.

Raatikainen, T., Brus, D., Hooda, R. K., Hyvarinen, A.-P., Asmi, E., Sharma, V. P., Arola, A., and Lihavainen, H.: Size-selected black carbon mass distributions and mixing state in polluted and clean environments of northern India, Atmos. Chem. Phys., 17, 371–383, doi:10.5194/acp-17-371-2017, 2017.

Ramanathan, V., and Carmichael, G.: Global and regional climate changes due to black carbon, Nat. Geosci., 1, 221-227, doi:10.1038/ngeo156, 2008.

Sahu, L. K., Kondo, Y., Moteki, N., Takegawa, N., Zhao, Y., Cubison, M. J., Jimenez, J. L., Vay, S., Diskin, G. S., Wisthaler, A., Mikoviny, T., Huey, L. G., Weinheimer, A. J., and Knapp, D. J.: Emission characteristics of black carbon in anthropogenic and biomass burning plumes over California during ARCTAS-CARB 2008, J. Geophys. Res., 117, D16302, doi:10.1029/2011JD017401, 2012.

Schwarz, J. P., Gao, R. S., Fahey, D. W., Thomson, D. S., Watts, L. A., Wilson, J. C., Reeves, J. M., Darbeheshti, M., Baumgardner, D. G., Kok, G. L., Chung, S. H., Schulz, M., Hendricks, J., Lauer, A., Karcher, B., Slowik, J. G., Rosenlof, K. H., Thompson, T. L., Langford, A. O., Loewenstein, M., and Aikin, K. C.: Single-particle measurements of midlatitude black carbon and light-scattering aerosols from the boundary layer to the lower stratosphere, J. Geophys. Res., 111, D16207, doi:10.1029/2006JD007076, 2006.

Schwarz, J. P., Gao, R. S., Spackman, J. R., Watts, L. A., Thomson, D. S., Fahey, D. W., Ryerson, T. B., Peischl, J., Holloway, J. S., Trainer, M., Frost, G. J., Baynard, T., Lack, D. A., de Gouw, J. A., Warneke, C., and Del Negro, L. A.: Measurement of the mixing state, mass, and optical size of individual black carbon particles in urban and biomass burning emissions, Geophys. Res. Lett., 35, L13810, doi:10.1029/2008GL033968, 2008.

Sirois, A., and Bottenheim, J. W.: Use of backward trajectories to interpret the 5-year record of PAN and O3 ambient air concentrations at Kejimkujik National Park, Nova Scotia, J. Geophys. Res., 100, 2867–2881, doi:10.1029/94JD02951, 1995.

Slowik, J. G., Cross, E. S., Han, J. H., Davidovits, P., Onasch, T. B., Jayne, J. T., WilliamS, L. R., Canagaratna, M. R., Worsnop, D. R., Chakrabarty, R. K., Moosmuller, H., Arnott, W. P., Schwarz, J. P., Gao, R. S., Fahey, D. W., Kok, G. L., and Petzold, A.: An inter-comparison of instruments measuring black carbon content of soot particles, Aerosol Sci. Technol., 41, 295–314, doi:10.1080/02786820701197078, 2007.

Stone, E. A., Schauer, J. J., Pradhan, B. B., Dangol, P. M., Habib, G., Venkataraman, C., and Ramanathan, V.: Characterization of emissions from South Asian biofuels and application to source apportionment of carbonaceous aerosol in the Himalayas, J. Geophys. Res., 115, D06301, doi:10.1029/2009JD011881, 2010.

Taylor, J. W., Allan, J. D., Allen, G., Coe, H., Williams, P. I., Flynn, M. J., Le Breton, M., Muller, J. B. A., Percival, C. J., Oram, D., Forster, G., Lee, J. D., Rickard, A. R., Parrington, M., and Palmer, P. I.: Size-dependent wet removal of black carbon in Canadian biomass burning plumes, Atmos. Chem. Phys., 14, 13755-13771, doi:10.5194/acp-14-13755-2014, 2014.

Vadrevu, K. P., Ohara, T., and Justice, C.: Air pollution in Asia, Environ. Pollut., 195, 233–235, doi:10.1016/j.envpol2014.09.006, 2014.

Virkkula, A., Makela, T., Hillamo, R., Yli-Tuomi, T., Hirsikko, A., Hameri, K., and Koponen, I. K.: A simple procedure for correcting loading effects of aethalometer data, J. Air Waste Manage. Assoc., 57, 1214–1222, doi:10.3155/1047-3289.57.10.1214, 2007.

Wan, X., Kang, S., Wang, Y., Xin, J., Liu, B., Guo, Y., Wen, T., Zhang, G., and Cong, Z.: Size distribution of carbonaceous aerosols at a high-altitude site on the central Tibetan Plateau (Nam Co Station, 4730 m a.s.l.), Atmos. Res., 153, 155–164, https://doi.org/10.1016/j.atmosres.2014.08.008, 2015.

Wang, Y. Q., Zhang, X. Y., and Draxler, R. R.: TrajStat: GIS-based software that uses various trajectory statistical analysis methods to identify potential sources from long-term air pollution measurement data, Environ. Modell. Softw., 24, 938–939, doi:10.1016/j.envsoft.2009.01.004, 2009.

Wang, M., Xu, B., Wang, N., Cao, J., Tie, X., Wang, H., Zhu, C., and Yang, W.: Two distinct patterns of seasonal variation of airborne black carbon over Tibetan Plateau, Sci. Total Environ., 573, 1041–1052, https://doi.org/10.1016/j.scitotenv.2016.08.184, 2016.

Wang, Q., Schwarz, J. P., Cao, J., Gao, R., Fahey, D. W., Hu, T., Huang, R. J., Han, Y., and Shen, Z.: Black carbon aerosol characterization in a remote area of Qinghai–Tibetan Plateau, western China, Sci. Total Environ., 479–480, 151–158, https://doi.org/10.1016/j.scitotenv.2014.01.098, 2014.

Wang, Q., Huang, R.-J., Zhao, Z., Zhang, N., Wang, Y., Ni, H., Tie, X., Han, Y., Zhuang, M., Wang, M., Zhang, J., Zhang, X., Dusek, U., and Cao, J.: Size distribution and mixing state of refractory black carbon aerosol from a coastal city in South China, Atmos. Res., 181, 163–171, https://doi.org/10.1016/j.atmosres.2016.06.022, 2016a.

Wang, Q., Huang, R.-J., Zhao, Z., Cao, J., Ni, H., Tie, X., Zhao, S., Su, X., Han, Y., Shen, Z., Wang, Y., Zhang, N., Zhou, Y., and Corbin, J. C.: Physicochemical characteristics of black carbon aerosol and its radiative impact in a polluted urban area of China, J. Geophys. Res. Atmos., 121, doi:10.1002/2016JD024748, 2016b.

Wang, Q. Y., Huang, R. J., Cao, J. J., Tie, X. X., Ni, H. Y., Zhou, Y. Q., Han, Y. M., Hu, T. F., Zhu, C. S., Feng, T., Li, N., and Li, J. D.: Black carbon aerosol in winter northeastern Qinghai-Tibetan Plateau, China: the source, mixing state and optical property, Atmos. Chem. Phys., 15, 13059–13069, doi:10.5194/acp-15-13059-2015, 2015a.

Wang, Q., Gao, R., Cao, J., Schwarz, J., Fahey, D., Shen, Z., Hu, T., Wang, P., Xu, X., and Huang, R.-J.: Observations of high level of ozone at Qinghai Lake basin in the northeastern Qinghai-Tibetan Plateau, western China, J. Atmos. Chem., 72, 19–26, doi: 10.1007/s10874-015-9301-9, 2015b.

Wang, Q., Zhao, Z., Tian, J., Zhu, C., Ni, H., Zhang, Y., Zhang, N., Shen, Z., Han, Y., and Cao, J.: Seasonal transport and dry deposition of black carbon aerosol in the Southeastern Tibetan Plateau, Aerosol Sci. Eng., doi:10.1007/s41810-017-0016-y, 2017.

White, W., Anderson, J., Blumenthal, D., Husar, R., Gillani, N., Husar, J., and Wilson, W.: Formation and transport of secondary air pollutants: ozone and aerosols in the St. Louis urban plume, Science, 194, 187–189, doi:10.1126/science.959846, 1976.

Wu, Y., Zhang, R., Tian, P., Tao, J., Hsu, S. C., Yan, P., Wang, Q., Cao, J., Zhang, X., and Xia, X.: Effect of ambient humidity on the light absorption amplification of black carbon in Beijing during January 2013, Atmos. Environ., 124, 217–223, https://doi.org/10.1016/j.atmosenv.2015.04.041, 2016.

Xu, B. Q., Cao, J. J., Hansen, J., Yao, T. D., Joswia, D. R., Wang, N. L., Wu, G. J., Wang, M., Zhao, H. B., Yang, W., Liu, X. Q., and He, J. Q.: Black soot and the survival of Tibetan glaciers, Proc. Natl. Acad. Sci. U. S. A., 106, 22114–22118, doi:10.1073/pnas.0910444106, 2009.

Yao, T., Ren, J., and Xu, B.: Map of glaciers and lakes on the Tibetan Plateau and the surroundings, Xi'an Cartographic Publishing House, 2008.

Yao, T., Thompson, L., Yang, W., Yu, W., Gao, Y., Guo, X., Yang, X., Duan, K., Zhao, H., Xu, B., Pu, J., Lu, A., Xiang, Y., Kattel, D. B., and Joswiak, D.: Different glacier status with atmospheric circulations in Tibetan Plateau and surroundings, Nat. Clim. Chang., 2, 663, 10.1038/nclimate1580, 2012.

Zhang, M., Wang, S., Li, Z., and Wang, F.: Glacier area shrinkage in China and its climatic background during the past half century, J. Geogr. Sci., 22, 15–28, doi:10.1007/s11442-012-0908-3, 2012.

Zhang, Q., Streets, D. G., Carmichael, G. R., He, K. B., Huo, H., Kannari, A., Klimont, Z., Park, I. S., Reddy, S., Fu, J. S., Chen, D., Duan, L., Lei, Y., Wang, L. T., and Yao, Z. L.: Asian emissions in 2006 for the NASA INTEX-B mission, Atmos. Chem. Phys., 9, 5131–5153, https://doi.org/10.5194/acp-9-5131-2009, 2009.

Zhang, R., Wang, H., Qian, Y., Rasch, P. J., Easter, R. C., Ma, P. L., Singh, B., Huang, J., and Fu, Q.: Quantifying sources, transport, deposition, and radiative forcing of black carbon over the Himalayas and Tibetan Plateau, Atmos. Chem. Phys., 15, 6205–6223, doi:10.5194/acp-15-6205-2015, 2015.

Zhang, X., Ming, J., Li, Z., Wang, F., and Zhang, G.: The online measured black carbon aerosol and source orientations in the Nam Co region, Tibet, Environ. Sci. Pollut. Res., 24, 25021–25033, 2017.

Zhang, Y., Kang, S., Li, C., Gao, T., Cong, Z., Sprenger, M., Liu, Y., Li, X., Guo, J., Sillanpää, M., Wang, K., Chen, J., Li, Y., and Sun, S.: Characteristics of black carbon in snow from Laohugou No. 12 glacier on the northern Tibetan Plateau, Sci. Total Environ., 607–608, 1237–1249, https://doi.org/10.1016/j.scitotenv.2017.07.100, 2017.

删除的内容: Wang, Q., Huang, R., Zhao, Z., Cao, J., Ni, H., Tie, X., Zhu, C., Shen, Z., Wang, M., Dai, W., Han, Y., Zhang, N., and Prévôt, A. S. H. : Effects of photochemical oxidation on the mixing state and light absorption of black carbon in the urban atmosphere of China, Environ. Res. Lett., 12, 044012, https://doi.org/10.1088/1748-9326/aa64ea, 2017.

Zhang, Y., Zhang, Q., Cheng, Y., Su, H., Kecorius, S., Wang, Z., Wu, Z., Hu, M., Zhu, T., Wiedensohler, A., and He, K.: Measuring the morphology and density of internally mixed black carbon with SP2 and VTDMA: new insight into the absorption enhancement of black carbon in the atmosphere, Atmos. Meas. Tech., 9, 1833–1843, doi:10.5194/amt-9-1833-2016, 2016.

Zhao, S., Ming, J., Xiao, C., Sun, W., and Qin, X.: A preliminary study on measurements of black carbon in the atmosphere of northwest Qilian Shan, J. Environ. Sci., 24, 152–159, https://doi.org/10.1016/S1001-0742(11)60739-0, 2012.

Zhao, S., Tie, X., Long, X., and Cao, J.: Impacts of Himalayas on black carbon over the Tibetan Plateau during summer monsoon, Sci. Total Environ., 598, 307–318, https://doi.org/10.1016/j.scitotenv.2017.04.101, 2017.

Zhao, Z., Wang, Q., Xu, B., Shen, Z., Huang, R., Zhu, C., Su, X., Zhao, S., Long, X., Liu, S., and Cao, J.: Black carbon aerosol and its radiative impact at a high-altitude remote site on the southeastern Tibet Plateau, J. Geophys. Res. Atmos., 122, doi:10.1002/2016JD026032, 2017.

Zhu, C.-S., Cao, J.-J., Xu, B.-Q., Huang, R.-J., Wang, P., Ho, K.-F., Shen, Z.-X., Liu, S.-X., Han, Y.-M., Tie, X.-X., Zhao, Z.-Z., and Chen, L. W. A.: Black carbon aerosols at Mt. Muztagh Ata, a high-altitude location in the Western Tibetan Plateau, Aerosol Air Qual. Res., 16, 752–763, doi:10.4209/aaqr.2015.04.0255, 2016.

Table 1. Trajectory clusters and mean refractory black carbon (rBC) concentration for each cluster.

Cluster	All trajectories			Polluted rBC trajectories[a]		
	Number	Mean	SD[b]	Number	Mean	SD
#1	421	0.37	0.71	120	0.95	1.14
#2	390	0.24	0.36	81	0.75	0.52
#3	76	0.32	0.31	23	0.72	0.29
All	887	0.31	0.55	224	0.86	0.90

[a]Trajectories associated with rBC concentration >0.33 μg m^{-3} (75th percentile value).

[b]SD represents standard deviation.

Figure Captions

Figure 1. Black carbon concentrations (μg m^{-3}) measured at 15 sampling sites on Himalayas and Tibetan Plateau based on the measurements from this study (blue solid circles) and other studies (black solid circles) from Ma et al. (2003), Pant et al., 2006, Marinoni et al. (2010), Stone et al. (2010), Babu et al. (2011), Engling et al. (2011), Zhao et al. (2012), Li et al. (2017), Wan et al. (2015), Wang et al. (2015a), Wang M. et al. (2016), Zhu et al. (2016), and Raatikainen et al. (2017). More detailed information concerning these studies is summarized in Table S1. The inset is a scatter plot of the mass concentrations of BC versus the altitude of each sampling site. The map in the figure was drawn using the Weather Research and Forecasting (WRF) model.

Figure 2. Time series plots of hourly-averaged refractory black carbon (rBC) mass concentrations, number fraction of thickly-coated rBC (F_{rBC}), mass median diameter of rBC particles (MMD), total suspended particulate matter (TSP), rBC/TSP, light absorption coefficient (b_{abs}), wind speed, wind direction (WD), and precipitation.

Figure 3. Diurnal variations of (a) refractory black carbon (rBC) mass concentrations, (b) planetary boundary layer (PBL) heights, (c) wind speeds, and (d) mass median diameters of the rBC particles (MMD). The lower and upper edges of the boxes denote the 25% and 75% percentiles, respectively. The short black lines and white circles inside the boxes indicate the median and mean values, and the vertical bars ("whiskers") show the 10th and 90th percentiles. LT stands for local time.

Figure 4. (a) Wind rose plot and (b) bivariate polar plot for the refractory black carbon (rBC) mass concentrations based on hourly data.

Figure 5. Time series plots of (a) wind vector ($= \frac{1}{n}\sum_{j=1}^{n} WS_j \times cos\theta_j$) and (b) surface transport intensity for refractory black carbon (rBC) based on the hourly-averaged data at the Lulang site. Positive values indicate the transport direction of rBC from south to north (i.e., from the Indo-Gangetic Plain and Bangladesh to Lulang) and the negative values represent the transport direction of rBC from north to south (i.e., from interior of the Tibetan Plateau) to Lulang.

Figure 6. Maps of (a) the mean trajectory clusters, (b) the concentration-weighted trajectories (CWT, μg m^{-3}) for refractory black carbon mass concentrations, and (c) the reconstructed black carbon column mass densities (kg m^{-2}) during the campaign.

Figure 7. Frequency distributions of mass median diameters (MMD) for rainy and non-rainy sampling days. The vertical dash lines denote the average MMDs for those two types of days.

Figure 8. (left panels) Diurnal variations of the hourly-averaged number fraction of thickly-coated refractory black carbon particles (F_{rBC}) and O_3 mixing ratios at Lulang and Qinghai Lake (QHL) and (right panels) linear regressions between F_{rBC} and O_3 at these two sites.

Figure 9. Frequency distributions of the mass absorption cross sections of refractory black carbon (MAC_{rBC}) for the campaign and for air masses defined by trajectory cluster.

Figure 10. Absorption enhancement (E_{abs}) versus (a) the number fraction of thickly-coated refractory black carbon (F_{rBC}) and (b) the mass median diameter (MMD) of rBC during the campaign. The error bars correspond to the standard deviations of E_{abs}, F_{rBC}, and MMD.